Experimental Evaluation of the Performance of Geomembrane Liners Subject to Downdrag and Seismic Loading

by

Angel Gutierrez

A Dissertation Presented in Partial Fulfillment
of the Requirements for the Degree
Doctor of Philosophy

Approved July 2016 by the
Graduate Supervisory Committee:

Edward Kavazanjian, Chair
Claudia Zapata
Jaewon Jang

ARIZONA STATE UNIVERSITY

August 2016

ABSTRACT

A series of experiments were conducted to support validation of a numerical model for the performance of geomembrane liners subject to waste settlement and seismic loading. These experiments included large scale centrifuge model testing of a geomembrane-lined landfill, small scale laboratory testing to get the relevant properties of the materials used in the large scale centrifuge model, and tensile tests on seamed geomembrane coupons. The landfill model in the large scale centrifuge test was built with a cemented sand base, a thin film Nafion^{TM} geomembrane liner, and a mixture of sand and peat for model waste. The centrifuge model was spun up to 60 g, allowed to settle, and then subjected to seismic loading at three different peak ground accelerations (PGA). Strain on the liner and settlement of the waste during model spin-up and subsequent seismic loading and accelerations throughout the model due to seismic loading were acquired from sensors within the model. Laboratory testing conducted to evaluate the properties of the materials used in the model included triaxial compression tests on the cemented sand base, wide-width tensile testing of the thin film geomembrane, interface shear testing between the thin film geomembrane and the waste material, and one dimensional compression and cyclic direct simple shear testing of the sand-peat mixture used to simulate the waste. The tensile tests on seamed high-density polyethylene (HDPE) coupons were conducted to evaluate strain concentration associated with seams oriented perpendicular to an applied tensile load. Digital image correlation (DIC) was employed to evaluate the strain field, and hence seam strain concentrations, in these tensile tests. One-dimensional compression tests were also conducted on composite sand and HDPE samples to evaluate the compressive modulus

of HDPE. The large scale centrifuge model and small scale laboratory tests provide the necessary data for numerical model validation. The tensile tests on seamed HDPE specimens show that maximum tensile strain due to strain concentrations at a seam is greater than previously suggested, a finding with profound implications for landfill liner design and construction quality control/quality assurance (QC/QA) practices. The results of the one-dimensional compression tests on composite sand-HDPE specimens were inconclusive.

DEDICATION

This dissertation is dedicated to my parents, Jose Angel and Margarita Gutierrez. Without their guidance and life lessons, I would not have been able to reach my professional goals.

ACKNOWLEDGMENTS

I would like to express my gratitude to my advisor, Edward Kavazanjian Jr., for being my mentor throughout all these years. His guidance and knowledge have been imperative to my success. He has been like a second father to me.

I would also like to thank Peter Goguen for all the help and guidance he has given me throughout the years. He was always there to help out and showed me a few new things along the way.

I would also like to thank all the staff at the UC Davis Center for Geotechnical Modeling. They always made me feel at home and were always more than happy to help when I hit a roadblock.

I want to thank Sean O'Donnell and Xuan Wu, my fellow classmates, for helping me at some point throughout my research.

Finally, I want to thank Jake Andresen. Without his help, I would have not been able get all testing done in a reasonable amount of time. His help and expertise in running DIC tests was of upmost importance to my work.

TABLE OF CONTENTS

Page

CHAPTER Page

LIST OF TABLES

Table Page

LIST OF FIGURES

Figure Page

Figure Page

Chapter 1

1 INTRODUCTION

1.1. Objective

The objective of the work described in this dissertation was to provide the physical data necessary to validate a numerical model developed by Arab (2011) for performance based design of geomembrane liners that are subject to large waste settlement and/or seismic loading. It is one part of a project with the global objective of evaluating the key factors influencing the performance based of geosynthetic liner systems for waste containment subject to extreme loading (large settlement and seismic loading), thereby enhancing environmental protection while facilitating more economical construction. This research is part of National Science Foundation (NSF) Project No. CMMI 1208026, "NEESR: Performance-based Seismic Design of Geomembrane Liner Systems for Waste Containment" (NSF Project). The research for this project was conducted at Arizona State University (ASU) and at the University of California at Davis Center for Geotechnical Modeling (UCD) under the U.S. National Science Foundation Network for Earthquake Engineering Simulation Research (NEESR) program.

The first phase of the project involved centrifuge testing at UCD. A physical model of a geomembrane-lined landfill was constructed and tested on the large UCD geotechnical centrifuge from which performance data were obtained for validation of the numerical model. The landfill model was spun up to 60 g and then subjected to an input design motion intended to simulate the 1994 Hyogo-ken Nanbu earthquake at three progressively increasing peak ground accelerations. Sensors were placed throughout the model to

measure geomembrane strain, seismic acceleration at key points of the model, and settlement of the simulated waste material. To account for the length scaling associated with centrifuge testing, a specialized 0.05 mm-thick Nafion^{TM} perfluorosulfonic acid/polytetrafluoroethylene (PFSA) membrane was used to model the liner in these tests. Specialized thin-film strain gages developed by Safaqah and Reimer (2006) were employed to measure membrane strains in this test. Block on an inclined plane tests were also conducted at UCD to obtain the interface shear strength between the PFSA membrane and the simulated waste material.

The second phase of the project involved smaller scale laboratory testing at ASU. These tests included conventional laboratory testing to get the properties of the materials used to construct the centrifuge model and specialized tensile testing of seamed geomembranes. The conventional testing included triaxial testing of the cemented sand material used for the base of the model, one-dimensional compression and cyclic simple shear testing of the sand-peat mixture used to simulate the waste, and tensile testing of the PFSA geomembrane. One-dimensional compression tests were also conducted on composite sand/HDPE specimens in an attempt to back calculate the geomembrane compressive stiffness. The specialized geomembrane testing consisted of tensile testing of seamed high density polyethylene (HDPE) geomembrane coupons to evaluate seam strain concentrations. Digital image correlation (DIC) was used to measure the strains on the geomembrane coupons.

1.2 Background

Current state-of-practice design procedures for geomembranes have proven to be inadequate for determining their performance when subject to waste settlement or seismic loads. Loads on a geomembrane due to waste settlement are often ignored in practice, though some engineers employ design details to minimize such loads. The current state-of-practice for seismic design of geomembranes is based upon Newmark seismic displacement analyses. However, Newmark analyses only provide an index of seismic performance and do not actually evaluate the strains and forces induced in the liner due to seismic loading. Furthermore, analyses conducted in accordance with current seismic design criteria cannot explain the tears that occurred in the liner of Chiquita Canyon Landfill as a result of the 1994 Northridge earthquake (Kavazanjian, et al. 2013). Therefore, a numerical model for explicitly evaluating the forces and strains in geomembrane liners subject to waste settlement and seismic loading was developed at Arizona State University (Arab 2011, Kavazanjian et al. 2014). This model includes the ability to account for relative displacement (slip) between the liner and adjacent materials during settlement or seismic loading, a particularly important and vexing issue. However, this numerical model lacks validation. Therefore, this research project was developed to help validate the numerical model and develop a more rational method for design of geosynthetic landfill liner systems subject to waste settlement and seismic loading as well as for other geosynthetic applications.

1.3 Organization of Dissertation Work

The contents of the work presented herein is divided into six chapters, including this introductory chapter that gives a brief overview of the research completed. Chapter 2 covers previous work that has an impact on the development of a more robust performance based design of geosynthetic liner systems for waste containment and on the experimental work presented in this thesis. Chapter 3 presents results of preliminary laboratory testing done to obtain information required prior to execution of the large scale centrifuge model test. Chapter 4 describes the large scale centrifuge test conducted at UC Davis of a model landfill with a geomembrane liner system and associated testing conducted at Arizona State University for the material properties for validation of the numerical model for performance based design of geomembranes developed at ASU. Chapter 5 describes the digital image correlation (DIC) analysis on seamed HDPE coupons to evaluate seam strain concentrations. Chapter 6 summarizes the work described in this thesis, presents the conclusions from the research conducted herein, and makes recommendations for future work that still has to be completed in order to properly validate the numerical model for performance based design of geosynthetic liner systems.

Chapter 2

2.0 BACKGROUND

2.1 Introduction

The purpose of this research program described in this dissertation is provide physical data necessary to validate a numerical model developed by Arab (2011) for performance based design of geosynthetic liner systems for waste containment. The data acquired for this purpose in the experimental program described herein is summarized in Table 2.1. Successful execution of the research program required building and testing a large-scale centrifuge model of a geomembrane-lined landfill, developing testing techniques for validation of geomembrane seam concentration factors, and testing of materials used in the centrifuge model to acquire necessary parameters for numerical model validation. This chapter reviews available techniques for accomplishing these objectives, provides the rationale for particular techniques chosen for use in this study, and provides additional background on the selected techniques.

Table 2.1. Summary of parameters acquired in the experimental program.

Parameter needed	Tests
Waste settlement	large scale centrifuge test
Waste mass accelerations	large scale centrifuge test
Geomembrane liner strains	large scale centrifuge test
Interface shear strength	tilt table tests
Geomembrane stiffness	1-D compression tests
Waste compressibility	1-D compression tests
Waste modulus and damping	cyclic simple shear tests
Foundation strength	triaxial compression tests
Foundation stiffness	1-D compression tests
Seam strain concentrations	geomembrane tensile tests

2.2 Current Practice for Accommodating Settlement

Current state-of-practice design procedures for geomembranes are inadequate for determining their performance when subject to waste settlement. Loads on a geomembrane due to waste settlement are often ignored in practice, though some engineers employ design details to minimize such loads. One solution that is applied in practice to minimize the tensile loads on a geomembrane due to waste settlement is use of a slip surface between the waste and the geomembrane liner. The slip surface acts as an isolator for the liner system. The force transmitted to the geomembrane is limited by the interface strength between the slip surface and the underlying material. Furthermore, if the interface strength on the bottom of the slip surface is less than that between the geomembrane and the underlying layer, no tension is transferred to the geomembrane as the waste settles. Though this may seem like a simple solution, it may present constructability and stability problems. Thus, it is not always possible to have a lower interface strength above the liner than below it. If the interface strength above the liner is higher than the interface strength below the liner, as settlement of the waste occurs tensile forces may be imparted by downdrag to the liner.

Fowmes (2007) and Fowmes et al. (2006) analyzed the impact of waste settlement on a geosynthetic lining system using the finite difference computer program FLAC^{TM}. Using FLAC^{TM}, two models were developed. The first model (model 1) looked at the full side slope of a landfill while the second model (model 2) focused on a single bench section for a more detailed approach to the effects of settlement and liner downdrag on liner performance. Fowmes (2007) and Fowmes et al. (2006) modeled many aspects of the

landfill construction and liner parameters that could affect liner system integrity due to settlement and downdrag. Some of the factors included in the models, as listed by Fowmes et al. (2006), include "strain dependent interface shear strength and axial strain behavior of the geomembrane, staged construction, and non-linear volumetric and shear behavior of the waste mass."

The lining system Fowmes et al. (2006) modeled was based on a large landfill in South East Asia that has signs of failure. The liner consisted of a drainage layer, a geomembrane, a protective geotextile, and a second drainage layer for leachate, as shown in Figure 2.1. Model 2 allowed Fowmes et al. (2006) to assess forces on the liner in detail. It also provided for a better representation of construction practices by allowing for waste lifts to be only 2 m thick. After the waste was built up to the height of the modeled bench, two 10 m lifts were placed on top of the waste to represent the loads induced by filling with waste over the next two benches. A pressure force was then applied to the surface of the waste to represent further waste lifts. Table 2.2 summarizes the geomembrane tensile stresses and strains obtained from the FLAC^{TM} analysis by Fowmes et al. (2006). Fowmes et al. (2006) concluded that even though models are out there that will help take into account waste settlement into liner design, current practice is far from developing a robust design procedure. The model developed by Fowmes et al. (2006) does not take into account waste degradation settlement and does not account for localized behavior of the geomembrane (or other geosynthetics) such as rupture and tearing of protection layers.

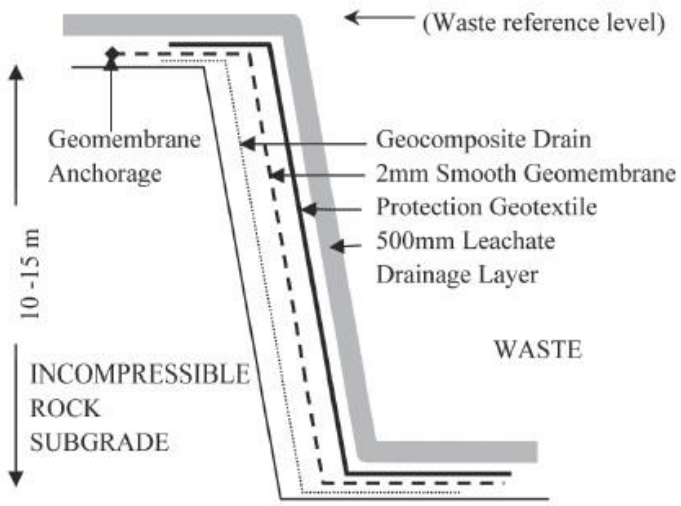

FIG. 2.1 Schematic of lining system used on rock benched subgrade (Fowmes et al., 2006)

Table 2.2. Axial strains and tensile forces in the geomembrane related to waste height for a southeast Asia landfill (Fowmes et al., 2006)

Waste height above bench.	Vertical pressure (kPa) at waste ref level	Maximum axial strain in geomembrane (%)	Maximum tensile stress in geomem-brane (kN/m)	Location of max stress (m below top of bench)
0	0	0.14	0.42	3.2
10	140	0.17	0.51	1.2
20	280	0.20	0.60	1.2
30	420	0.20	0.59	1.2
40	560	0.37	1.32	2.4
50	700	0.40	1.43	4.8
60	840	8.37	25.1	3.6
70	980	14.7	44.9	1.2

Thiel et al. (2014) presented a method for design of geosynthetic liner systems on the side slopes of landfills using a slip layer to mitigate downdrag forces. The method they describe for mitigating the tensile forces due to downdrag using a slip element is illustrated

in Figure 2.2. The slip element illustrated was a geonet with a low interface strength on the bottom side. The geonet was underlain by a high strength geotextile over the upper part of the slope on the bench and below the crest of the bench, where tensile stresses due to downdrag would be the highest. The underlying high-strength geotextile would sustain the tensile forces induced by downdrag and mitigate the tensile forces on the primary geomembrane.

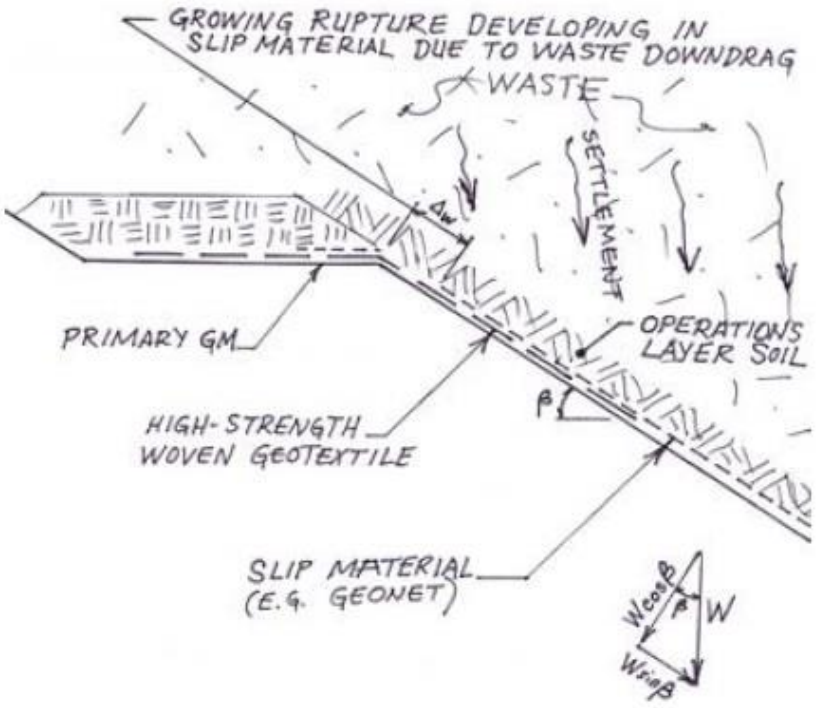

FIG 2.2. High-strength geotextile protecting primary geomembrane after slip element ruptures due to downdrag (Thiel et al., 2014)

Thiel et al. (2014) also employed the finite FLAC^{TM} difference model of Arab (2011) to look at the effects of downdrag and settlement on a geomembrane liner. Their model consisted of a geosynthetics-lined landfill with 1H:1V slopes on one side and 2H:1V

on the other side. Each side of the landfill had three 12.3 m-high segments separated by 4 m-wide benches. The interface strength on top of the geomembrane was characterized by a friction angle of 30 degrees and the interface strength below the geomembrane was characterized by a friction angle of 10 degrees. The waste material was modeled using the Cam-Clay constitutive model and an approach to model waste settlement developed by Arab (2011). Waste placement was simulated by first placing the waste in lifts using a typical value for waste compressibility and then, at the end of waste placement, the compressibility of the waste was changed such that a total settlement equal to 17% of the waste thickness was induced at the center of the model, thereby mimicking the long-term settlement due to waste degradation. Thiel et al. (2014) report the vertical settlement and downslope displacement at three points along each slope in the model. These settlements and displacements are presented in Table 2.3.

Table 2.3. Vertical settlement and relative slope displacement at the crest of each slope segment for frictionless slopes (Thiel et al., 2014)

	1H:1V Slope			2H:1V Slope		
	Lower Slope	Middle Slope	Upper Slope	Lower Slope	Middle Slope	Upper Slope
Vertical settlement	2.00 m	1.78 m	0.65 m	1.20 m	0.40 m	0.21 m
Slope displacement	2.83 m	2.52 m	0.92 m	2.68 m	0.89 m	0.47 m

Theil et al. (2014) also reported the maximum tensile force that the geomembrane liner was subjected to due to waste downdrag. The tensile forces are presented in Figure 2.3. Note that the strains on the geotextile on the 1H:1V slope are much higher than those seen on the 2H:1V slope.

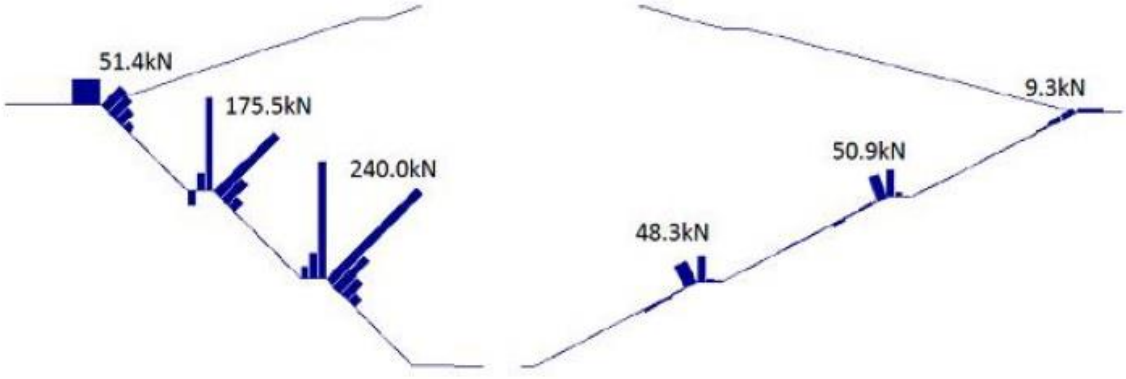

FIG 2.3. Tensile forces (per meter) induced in the high strength geotextile by downdrag (Thiel et al. 2014)

The results from the analyses show that the tensile forces induced on the geotextile by waste settlement are typically below the yield strength of geomembranes currently available except for steep side slopes. However, it must be noted seismic loading can apply additional tensile strain to a geomembrane liner.

It can be seen from the work mentioned above that tensile strain due to downdrag can be a problem under some conditions, and that numerical analyses can be used to predict tensile forces. However, these analyses must be validated.

2.3 Field Performance of Geosynthetic Liners

The field performance of geosynthetic landfill liners has not been extensively studied due to constraints such as the frequency of event occurrence, lack of instrumentation in or around the landfill area, and lack of co-incidence of significant earthquake and lined landfill locations. Due to lack of instrumented case histories, it has

been difficult to properly evaluate the current design methods for seismic design of geosynthetic landfill liners. However, the performance of geosynthetic-lined landfills in earthquakes has been evaluated based upon post-earthquake observations, strong motion records from locations near affected landfills, and post-earthquake performance analyses. There is also one case where instrumentation at the landfill documented waste response, the performance of the Operating Industries, Inc. (OII) landfill in the 1994 Magnitude 6.7 Northridge earthquake in California. However, the OII landfill was not a lined facility.

Augello et al. (1995) looked at the performance of landfills affected by the Northridge earthquake. Overall, most of the geomembrane-lined landfills that were subjected to strong ground motions in the Northridge event were observed to have performed well under the seismic loads. However, one geomembrane-lined landfill did have significant damage. Two tears were observed in the geomembrane liner at the Chiquita Canyon landfill in post-earthquake inspections. These tears are documented in a forensic study conducted by EMCON (1994).

Kavazanjian et al. (2013) evaluated the performance of the Chiquita Canyon Landfill in the 1994 Northridge earthquake. They concluded that the current state-of-practice of Newmark analyses did not accurately predict tears in the geomembrane at Chiquita Canyon. They also employed the two-dimensional non-linear finite difference model of Arab (2011) to evaluate the Chiquita Canyon landfill liner. However, the strains in the geomembrane at Chiquita Canyon predicted by the Arab (2011) numerical model were less than the yield strain of the geomembrane. Kavazanjian et al. (2013) could only explain the tears in the Chiquita Canyon geomembrane by invoking strain concentration

factors from Giroud (1995, 2005) for seams and scratches oriented parallel to an applied tensile load.

2.4 Current Practice for Seismic Design of Liners

Current practice for seismic design of geomembrane liners is based upon decoupled seismic response analysis, in which the response of the waste is decoupled from the potential for slip at the liner interface, and a Newmark seismic displacement analysis (Newmark 1965) in which the response of the waste mass is then used to calculate slip at the liner interface. The calculated displacement is compared to limiting displacements based upon comparison of decoupled Newmark analysis results to the observed performance of landfills (Augello et al., 1995). A calculated displacement of 150 mm is generally assumed to be indicative of no damage to a geomembrane.

Bray et al. (1998) discuss the necessary aspects that should be included into a proper methodology for seismic design of geosynthetic liner systems. These aspects include the properties of the waste and the liner material, a non-linear seismic response analysis, and a seismic stability evaluation. They note that investigators developing seismic design procedures for landfill liner systems should look at case histories such as the performance of the Chiquita Canyon and Lopez Canyon landfills in the Northridge earthquake to draw necessary lessons from them. Bray et al. (1998) developed a simple two-stage seismic analysis procedure for landfill design based upon non-linear seismic response analysis and Newmark displacement analysis. In the Bray et al. (1998) analysis, the free field peak ground acceleration at the landfill site (termed the maximum horizontal acceleration, or

MHA) is used to evaluate the maximum horizontal equivalent acceleration (MHEA) for the potential failure mass based upon the characteristics of the earthquake motion (e.g., its fundamental period), the fundamental period of the waste mass, and a non-linear response factor. The seismic displacement is then evaluated based upon the ratio of the MHEA and the yield acceleration of the system and the earthquake magnitude. Bray et al. (1998) note that the variability in native soil and waste properties can be a challenge in proper design since they affect the dynamic response and non-linear response of the landfill.

Matasovic and Kavazanjian (2006) compared four different analytical methods for seismic performance of landfill covers when looking at the performance of the Olympic View Sanitary Landfill (OVSL) during the February 2001 Nisqually earthquake. They evaluated the performance of the geosynthetic cover system at the site using each of the four methods, and then compared the results of their analysis to the observed performance of the cover liner system. Note, however, that no damage was observed to the OVSL cover system in this earthquake, limiting the conclusions that could be drawn from these analyses.

The first two methods used by Matasovic and Kavazanjian (2006) were chart solutions that are included in the United States Environmental Protection Agency (EPA) guidance document for seismic design of solid waste landfills (Richardson et al. 1995). The third method, which was mentioned above, was the more robust procedure developed by Bray et al. (1998). The fourth and final method was the conventional decoupled equivalent-linear site response/Newmark-type permanent seismic deformation method developed in which the seismic response analysis is an equivalent-linear analysis and that does not consider slip at the liner interface.

Matasovic and Kavazanjian (2006) noted that each of the four methods used the same general procedure that consisted of three steps: evaluating the yield acceleration of the waste-mass liner system; evaluating the peak horizontal acceleration at the top of the landfill and the peak average acceleration or the average acceleration time history of the waste mass; and using yield acceleration and either the peak average acceleration or the acceleration time history (depending on method) to calculate the seismically induced permanent displacement. Matasovic and Kavazanjian (2006) concluded that methods 1 and 2 are very conservative but still predicted the observed good performance of the OVSL cover system. They also noted that if methods 1 and 2 resulted in a deformation greater than 300 mm it did not necessarily mean the cover would not perform well due to the very conservative assumptions embodied in both methods but would merely indicate that a more sophisticated analysis was needed. Method 3 was more refined than Method 1 and 2, however this method was still conservative. Matasovic and Kavazanjian (2006) noted that the refinements in Method 3, which required additional computational effort, should help provide something closer to the behavior observed on the field. Finally, Method 4 was considered to be the most consistent with the observed performance seen of the OVSL cover system.

Kavazanjian et al. (2013) present the case history of the performance of the liner systems in Canyons C and D at the Chiquita Canyon Landfill in the Northridge earthquake. State-of-practice Newmark displacement analyses conducted after the earthquake suggest that the liner system in both Canyons should have performed. Because State-of-Practice Newmark analysis failed to predict the damage to the Chiquita Canyon liner system, and

because Newmark analysis is merely an index of seismic performance, Kavazanjian et al. (2013) conclude that the current state of practice for seismic design of geomembrane liners is not adequate.

2.5 Performance Models of Geosynthetic Liner Behavior

Fowmes (2007) developed a FLAC^{TM} (Itasca, 2008) model for the performance of geomembrane liner systems subject to waste settlement. In this model, geosynthetic materials are modeled as linear elastic beam elements with zero moment of inertia and with elastic-perfectly plastic interface elements on both sides. Interface strength is described by a Mohr-Coulomb type failure criterion. To validate his model, Fowmes (2007) applied it to the analysis of laboratory scale behavior of geosynthetic lining systems and the model was considered to provide an appropriate representation of measured observations. Fowmes (2007) then applied his model to investigate the performance of geosynthetic liner systems in steep-sided quarry landfills. Fowmes et al. (2006) applied the Fowmes (2007) model to predict a lining system integrity failure in a steep sided landfill in Hong Kong.

Arab (2011) built on the Fowmes (2007) FLAC^{TM} model described above. Arab (2011) used all of the features used by Fowmes (2007) in modeling the liner system, including modeling the geomembrane as a beam element with zero moment of inertia. Arab (2011) added a non-linear stress-strain model for geomembranes that was developed by Giroud et al. (1995) to the geomembrane element. Arab (2011) also included a hysteretic interface stress-strain law with post-peak strain softening to model geosynthetic clay liners in his FLAC^{TM} model to model seismic loading.

Kavazanjian et al. (2012) described the use of the Arab (2011) FLAC^{TM} model for performance based seismic analysis and design model of geosynthetic waste containment systems. The improvement of this model over state-of-practice Newmark analysis-based procedures is that it allows for explicit calculations of strains and forces in the geomembrane liner system. Kavazanjian et al. (2012) showed that the model accurately predicted behavior of a rigid block on a horizontal plane and gave reasonable results for forces and strains in the geosynthetic liner systems. One important conclusion that must be noted from Kavazanjian et al. (2012) is the need to validate the model through physical testing (due to lack of appropriate case history data).

Wu (2013) demonstrated the ability of the Arab (2011) FLAC^{TM} model to predict tensile forces and strains in side slope liner geomembranes subject to large waste settlement. The analyses conducted by Wu (2013) showed that the magnitude of the tensile forces and strains induced by waste settlement depended on the difference between the interface strength on top of the geomembrane and the interface strength beneath the geomembrane. When the interface strength on top of the geomembrane was less than the interface strength beneath the geomembrane, little to no tension was induced in the geomembrane. When the interface strength above the geomembrane was greater than the interface strength beneath the geomembrane, the magnitude of induced tensile strain and force increased as the difference between the upper and lower interface strength increased. The analyses conducted by Wu (2013) also showed that: 1) tensile strains are greatest on bencher where the geomembranes are anchored and near the crest of the side slope just below the bench; 2) the geomembrane at the toe of the slope is put into compression by

waste settlement; 3) the magnitude of tensile strains a d forces increase as the slope angle increases from 3H:1V (Horizontal:Vertical) to 2H:1V to 1H:1V. While the results obtained by Wu (2013) appear to be reasonable, once again there is no physical data to validate these analyses.

2.6 Physical Model Testing

Due to the absence of appropriate field case history data, physical model testing must play an essential role in validating the Arab (2011) numerical model and the findings of Wu (2013) and Kavazanjian et al. (2013). This section discusses the physical model testing methods employed in this dissertation to provide data that can be used to validate the numerical model of Arab (2011).

2.6.1 Centrifuge Testing

Centrifuge testing has been employed to test scale models of geotechnical systems for over 40 years. The advantage of centrifuge testing is that field-scale stresses can be applied to small scale models in the laboratory. To understand how geotechnical centrifuge testing can be used to mimic field conditions, centrifuge scaling laws must be understood. Kutter (1992) explains the principle of scaling laws in centrifuge testing in a simple fashion. As a model is spun up to a centrifugal acceleration of N times g, where g is the acceleration of gravity at the earth's surface, the dimensions of the model, are scaled by a factor of N, i.e. the prototype dimension is N times the dimensions of the model, and the pressures and stresses in the model increase by the same factor N. Therefore, the

relationship of the model stress to the field, or prototype, stresses can be expressed mathematically by Equation 2.1:

$$\sigma^* = \frac{\sigma_{model}}{\sigma_{prototype}} = 1 \qquad (2.1)$$

where σ is stress, prototype refers to actual conditions, and the asterisk denotes the centrifuge model scale factor (Kutter 1992). Thus, in a centrifuge model length is scaled down, gravity is scaled up by the same factor, and stress remains the same. Note that under these conditions mass density in the model remains the same as in the prototype. Scaling factors for other parameters such as earthquake acceleration must also be considered in centrifuge testing. Table 2.4 contains the most common scaling factors for geotechnical centrifuge model testing.

Table 2.4. Scale factors for centrifuge model tests (Kutter, 1992).

Quantity	Symbol	Units	Scale Factor
Length	L	L	$1/N$
Volume	v	L^3	$1/N^3$
Mass	m	m	$1/N^3$
Acceleration, Gravity	a, g	L/T^2	N
Force	F	mL/T^2	$1/N^2$
Stress	σ	m/LT^2	1
Moduli	E	m/LT^2	1
Strength	s	m/LT^2	1
Time (dynamic)	t_{dyn}	T	$1/N$
Frequency	F	$1/T$	N
Time (diffusion)[a]	t_{dif}	T	$1/N^2$

2.6.2 Interface and Base Isolation Testing of Geosynthetics

A significant amount of research has been conducted on the use of geosynthetics for base isolation of structural systems. The tests usually have involved a simple rigid block on a plane test in a centrifuge or 1-g shake table setting. One or more geosynthetic materials are placed between the block and plane to frictionally base isolate the block. A representative motion is then applied to the system, and the response of the block is measured in comparison to the response of the base or plane. Base isolation is achieved by providing a low interface friction angle between the block and the plane, limiting the transmitted earthquake acceleration to the tangent of the interface friction angle (assume no adhesion). Kavazanjian et al. (1991) describe these types of block on a plane tests for both 1-g shake table and centrifuge testing. These investigators studied base isolation system between a variety of geomembrane/geotextile interface and a layered geomembrane/geotextile/soil layer systems. Kavazanjian et al. (1991) concluded that a geosynthetic material with a smooth surface can effectively be used as a frictional base isolation system.

Yegian et al. (1999) also ran shake table tests to study the use of geosynthetics as a frictional base isolation system. Yegian et al. (1999) concluded that the use of a geosynthetic interface was a much more cost effective way of reducing the dynamic response of buildings than other types of base isolation systems. Yegian et al. (1999) concluded that the shear force on a geosynthetically-isolated base isolated structure could be limited to as little as 35% of that observed in a standard fixed structure. The findings of Yegian et al. (1999) was in agreement with those of Kavazanjian et al. (1991) with

regard to the effectiveness of geosynthetics base isolation as a way of reducing dynamic response of structural systems.

Wartman et al. (1999) also conducted both block on a plane and soil column tests with geosynthetic interfaces between the block or soil column and the plane. Wartman et al. (1999) concluded that the Newmark rigid block assumption is unconservative when the excitation frequency is less or equal to the natural frequency of the soil column. If the excitation frequency is much greater than the natural frequency of the soil column, the Newmark rigid block assumption turns out to be accurate or conservative. The results of Wartman et al. (1999) show that the natural frequency of the material system and the frequency content of the earthquake ground motions must be considered when contemplating the use of a geosynthetic base isolation system.

Kavazanjian et al. (1991), Yegian et al. (1999), Wartman et al. (1999), Wartman et al. (2001), and Wartman et al. (2005) all show that relative displacement (slip) at a geosynthetics interface creates a non-linear dynamic response and changes the dynamic response of the structure above the geosynthetic interface.

2.6.3 Centrifuge Testing of Landfill Models

The absence of any instrumented case histories of landfills with geosynthetic liner systems makes physical model testing the only choice for validating a numerical model of the seismic behavior of such systems. However, creating a physical model of a landfill at prototype scale is impractical due to the sheer size of a landfill. Therefore, researchers have turned to centrifuge testing as a solution. As mentioned before, centrifuge testing allows

for the use of scale models. For example, a 40-foot-high slope on a landfill can be modeled by creating a 1-foot-high model of the slope and spinning up to 40 g in the centrifuge. In order to build a proper model for centrifuge testing, the materials used in the model have to mimic the actual materials used in the field. Due to scaling laws, use of actual materials used in the field may not be possible. For instance, if the actual waste material was used in a centrifuge test a twig, once spun up to a 40g centrifugal acceleration, would turn into a large tree trunk.

Thusyanthan et al. (2005a) conducted laboratory testing to develop a material that would exhibit the mechanical properties of a typical municipal solid waste material in the field. These investigators tested three different peat:clay:sand model waste mixtures: a 2:1:1 mixture (Mix A), a 1:1:1 mixture (Mix B), and a 1:2:1 mixture (Mix C). They evaluated the unit weight, compressibility, shear strength, and particle size distribution of these mixes as well as their ease of handling. Thusyanthan et al. (2005a) concluded that Mix B, which was 1 part peat, 1 part clay, and 1 part sand, was the best option for modeling waste in centrifuge tests. This material was then employed in a dynamic centrifuge model test of a landfill (Thusyanthan et al., 2005b).

Thusyanthan et al. (2005b) conducted two centrifuge tests using the model waste material developed in Thusyanthan et al. (2005a). In the first test, the shear wave velocity and the settlement of the model waste was monitored throughout the test. In the second test, the dynamic response of the model waste was monitored. The results from the dynamic response of the model waste were also used to develop modulus reduction and damping curves of the model waste. Thusyanthan et al. (2005a) concluded that the model

waste exhibited similar settlement and dynamic characteristics as those seen from municipal solid waste in the field.

2.7 Strain Gages

Data for numerical validation of a numerical model for performance based design of geosynthetic liner systems using physical model testing includes the strain induced on the geomembrane liner during the physical model tests. Since the geomembrane is flexible, a typical strain gage sensor cannot be used for this purpose

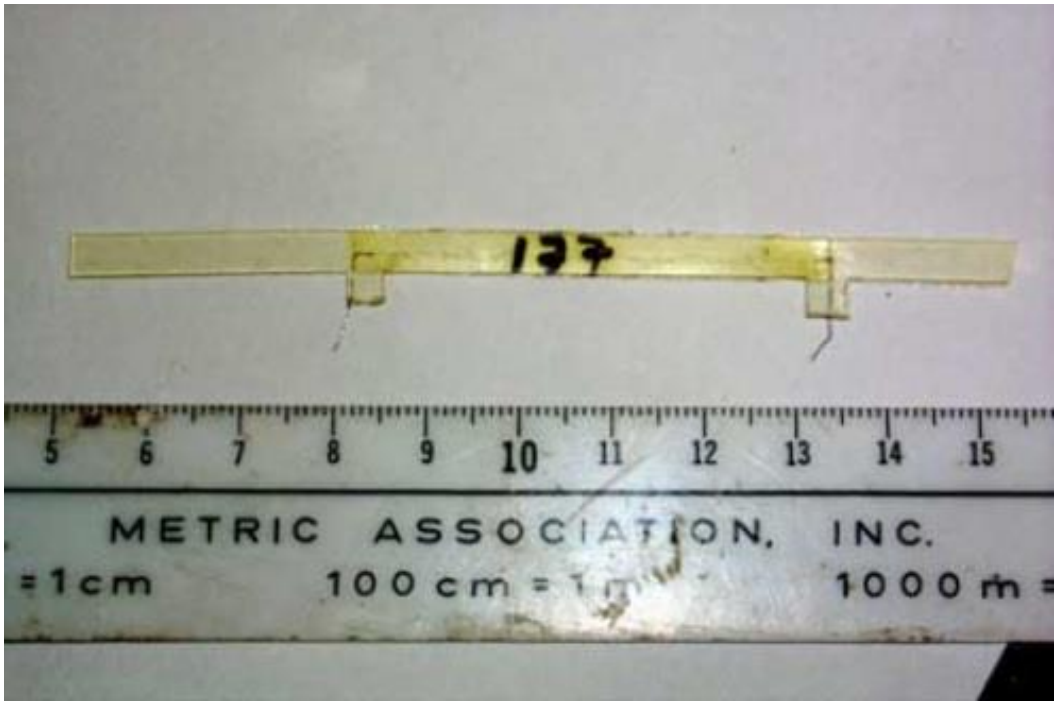

FIG 2.4. A picture showing the elastomer gage. (Safaqah and Riemer 2006)

Safaqah and Riemer (2006) developed flexible strain gages for measuring strains of a flexible membrane, e.g., a latex membrane used in a triaxial compression test that can

accurately measure small, localized strains within a range of 0.0005% to 10%. The strain gages, as shown in figure 2.4, consists of a polyurethane body which houses a liquid metal alloy within it. As the polyurethane body stretches, the liquid metal alloy "stretches" along with it. The extension of the metal alloy changes the resistance of the circuit completed by the alloy, which can then be translated into a measurement of strain. These strain gages can be easily adhered to plastic, which allows their use in centrifuge testing of geomembranes.

2.8 Strain Concentration Factors

Arab (2011), and later Kavazanjian et al. (2012) and Kavazanjian et al. (2013), employed a performance based finite difference model to analyzed tears in the Chiquita Canyon landfill liner system during the 1994 Northridge earthquake. In order to explain these tears, i.e., in order to show the strain in the geomembrane exceeded the yield strain of the geomembrane, the strain concentration factors for seams and scratches in geomembranes when oriented perpendicular to an applied tensile load developed by Giroud et al. (1995) had to be invoked.

The Giroud et al. (1995) seam strain concentration factors are based the following mechanism. When two pieces of geosynthetic that are not perfectly co-planar are stretched in tension, there is a bending moment induced along the seam, as seen in figure 2.5. The maximum bending strain is along the bending inflection points and represents an "amplification" of average tensile strain within the geosynthetic. The maximum bending strain is composed of the average tensile strain plus an additional incremental tensile strain.

Therefore, there is an incremental strain that is equal to the bending strain plus the tensile strain.

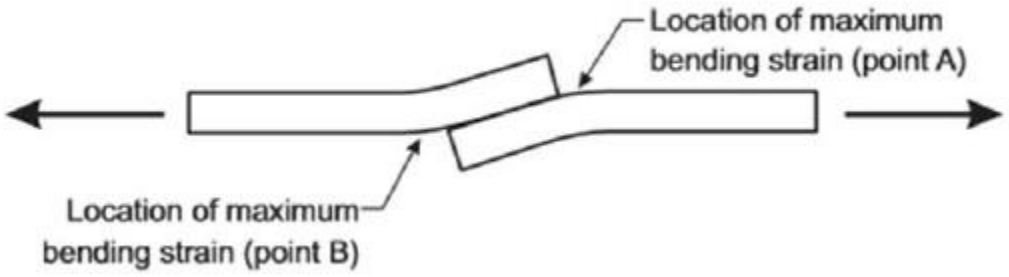

FIG 2.5. Geomembrane bending on each side of seam (Giroud, 2005).

Giroud (2005) presented a series of plots of incremental bending strain vs. average tensile strain for different types of geomembrane seams. The additional strain that occurs due to the bending strain varies depending on seam type, seam width, geomembrane thickness, and seam thickness. Figure 2.6 shows an example of the plots developed by Giroud (2005) that were developed based upon his previous work presented in Giroud et al. (1993) and Giroud (1995). The Giroud strain concentration factors are based upon theoretical considerations: no physical testing has been conducted to validate the strain concentration factors developed by Giroud.

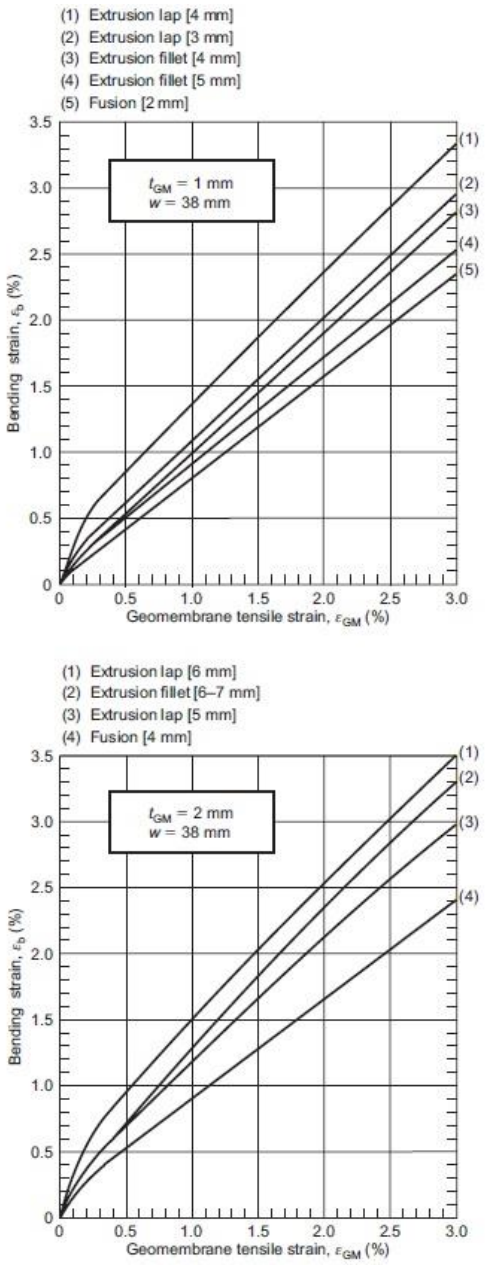

FIG 2.6 Additional strain due to geomembrane bending next to a seam, ε_b, as a function of the tensile strain in the geomembrane away from the seam, ε_{gm} (Giroud et al. 1993, 1995) (Notes: The value indicated in square brackets is the total seam thickness, which is thickness of the extrudate, if any, plus thickness of two geomembrane layers. Notations: t_{GM}= geomembrane thickness; w = seam width.) (Giroud 2005).

Chapter 3

3.0 PRELIMINARY TESTING

3.1 Introduction

This chapter describes preliminary stand-alone tests conducted prior to the large scale centrifuge tests that were required to facilitate the centrifuge testing program.

3.2 Adhesive Selection

3.2.1 Introduction

One of the obstacles identified during the planning stage for the centrifuge model tests an adhesive for the attachment of various materials (e.g., thin film polymer strain gages) to geosynthetic polymeric materials. The need to find a proper adhesive was imperative. The adhesive had to work with a perfluorosulfonic acid/polytetrafluoroethylene (PFSA) membrane, polyurethane, and possibly with high density polyethylene (HDPE). The main consideration was the adhesion of polyurethane to PFSA. This was due to the fact that the geomembrane used in the large scale centrifuge was composed of PFSA, while the thin film strain gages used to monitor strains in the centrifuge tests were made with polyurethane. Therefore, tests were conducted to identify an appropriate adhesive. Three different adhesives were tested: Loctite® Super Glue Plastics Bonding System with Activator, Loctite® Epoxy Plastic Bonder, and Loctite® Super Glue Liquid Professional.

3.2.2 Testing Method and Results

A very simple method was used to determine which adhesive would work best. The ends of three damaged strain gages were attached to a small piece of PFSA. The other end of the strain gages was not attached to the PFSA membrane and was allowed to float freely. Each strain gage was attached using a different adhesive. The adhesives were allowed to cure for a day, then tested. The test consisted of pulling on the floating end of the strain gage until failure occurred. Failure consisted of detachment from the PFSA membrane or tear in either the membrane or the strain gage. Once all three strain gages exhibited failure, the testing procedure was complete.

Results were very different for each of the adhesives tested. The super glue seemed to be the least effective. As soon as there was a small amount of load applied to the attachment point, the strain gage came right off. In the cases of both the epoxy and the plastic bonding system the strain gage tore before it detached from the PFSA membrane, indicating the bond was stronger than the strain gage material. However, the application of epoxy was not as clean as the application of the plastic bonding system and led to a thicker attachment point. Since the point of instrumenting the PFSA membrane with the thin film strain gages was to minimize strain gage influence on the behavior of the membrane, the plastic bonding system was selected. Two more tests were conducted with the plastic bonding system, and the outcome was always the same. Therefore, the Loctite® Super Glue Plastics Bonding System with Activator was chosen to as the preferred adhesive for attachment of the strain gages to the PFSA membrane.

3.3 One-Dimensional Compression Tests on HDPE

3.3.1 Sample Preparation

In order to evaluate the compressive modulus of HDPE, one-dimensional compression tests were conducted. Due to the potential for buckling of HDPE when subjected to compressive loading, a testing method that avoided the potential for buckling was developed. In this method, a 5 mm diameter HDPE resin cord with the same height as an oedometer ring (in our case 1 in high), was placed in the center of the oedometer ring. The surrounding area was then filled with Ottawa 20/30 at a density close to 100% relative density (i.e. 95-99%). This created an anisotropic, non-buckling composite sand/HDPE sample that could be subjected to a one-dimensional compression test. Figure 3.1 shows a diagram of the sample.

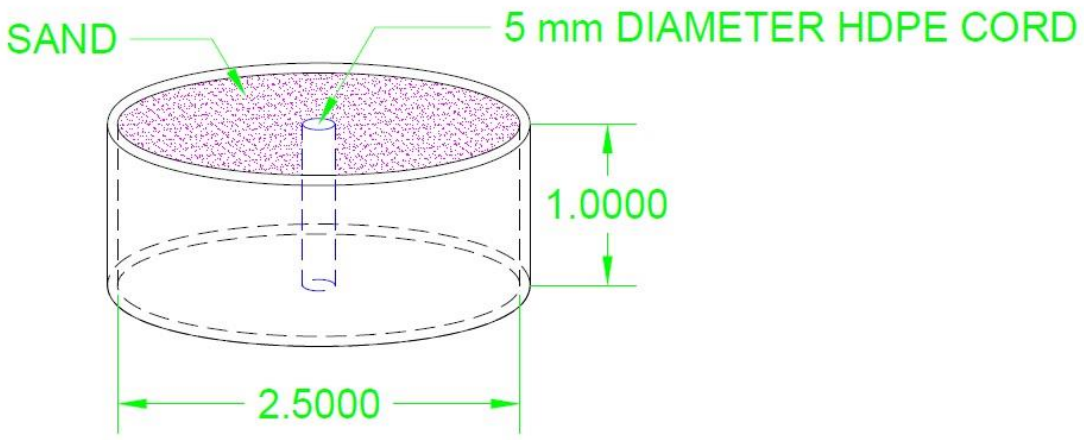

FIG 3.1. Diagram of HDPE/sand composite sample.

One-dimensional compression tests of Ottawa 20/30 at relative densities between 95-99% were also conducted. The purpose of this was to have a comparison between the HDPE/sand samples and the sand samples. The comparison would allow us to detect differences, and in turn back calculate the compressive modulus of HDPE.

3.3.2 Test Procedure

The test employed for evaluating the compressive modulus of HDPE consisted of a conventional one-dimensional compression test. The composite sample was placed in the one-dimensional compression apparatus illustrated in Figure 3.2. Loads of 50, 250, 500, 1000, 2000, 4000, and 8000 psf were then applied to the sample. After each applied load, the sample was allowed to settle. Once no significant movement was seen, the next stage of loading was applied. Once all the stages of loading were completed, the sample was removed from the apparatus. No rebound analysis was conducted on the tests since it was not necessary for the purpose of this project.

One-dimensional compression tests of specimens composed only of Ottawa 20/30 sand at relative densities between 95-99% were also conducted. The purpose of these tests was to provide data for comparison to the composite HDPE/sand samples and the sand samples. The intent was that differences between the two types of tests would allow for calculation of the compressive modulus of HDPE.

FIG 3.2. One-dimensional compression test apparatus.

3.3.3 One-Dimensional Compression Test Results and Discussion

Figure 3.3 shows the results of the compression tests on both the sand and composite HDPE/sand samples. Tests with a P designation are on specimens with HDPE cords in them, while the ones without a P designation are the Ottawa 20/30 sand tests. From figure 3.3, we can see that while there is a difference between the initial loading of the samples (seating load), there is no real difference after the initial loading of the samples. The curves have very similar slopes after initial loading, which leads to the conclusion that

there is little to no difference between the compressibility of the sand and the sand/HDPE samples.

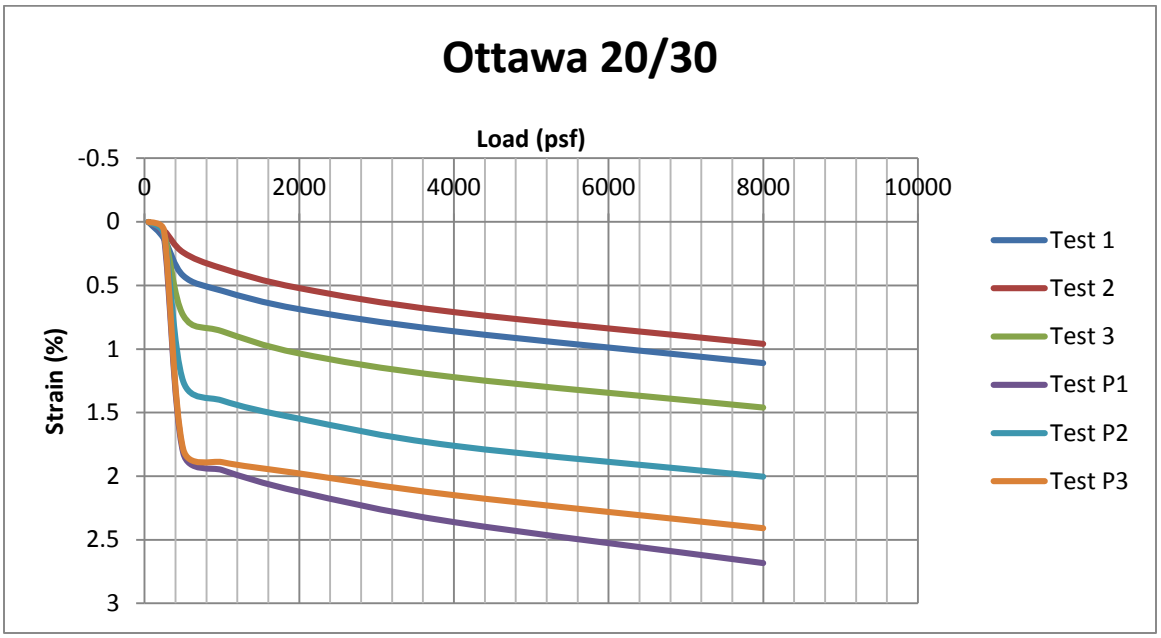

FIG. 3.3. One-dimensional Compression Test Results.

3.3.4 Conclusions and Future Work

One-dimensional compression tests were conducted on sand and composite sand/HDPE samples in an attempt to evaluate the compressive modulus of HDPE. A total of six tests were run, three on sand and three on composite HDPE/sand samples. The results showed little difference in the compressibility of the two types of specimens. One possible reason for this is that the compressibility of HDPE is close to the compressibility of dense sand. The difficulty of creating the HDPE/sand samples, the variability of the relative density of the sand, the seating of each sample, could also have contributed these

results. The author suggests that a better testing method for evaluating the compressibility of HDPE should be developed.

3.4 Tilt Table Tests on PFSA Membrane

The shear strength of the geomembrane/waste material interface is an important factor in the numerical modeling of the large scale centrifuge test. A simple tilt-table test was conducted to obtain a preliminary measurement of interface strength. Note that small centrifuge tests were run by Wu (2016) for frequency-dependent interface strength and stiffness values for the interfaces used in the model.

The tilt table test setup employed a PFSA membrane rigidly attached to a wood board. A small "fence" box made of polytetrafluoroethylene (PTFE) was placed on top of the PFSA membrane. The box was then filled with the simulated waste material that was to be used in the centrifuge test. The board was then slowly tilted until slip of the box was observed. The angle at the moment of slip was recorded, and the test was repeated three times. The average angle at which slip initiated in the three tests of 26.7° was considered to be representative of the interface shear strength friction angle between PFSA and the simulated waste.

Chapter 4

4.0 LARGE SCALE CENTRIFUGE TEST OF A GEOMEMBRANE-LINED LANDFILL SUBJECT TO WASTE SETTLEMENT AND SEISMIC LOADING

4.1 Abstract

A large scale centrifuge test of a geomembrane-lined landfill subject to waste settlement and seismic loading was conducted to help validate a numerical model for performance based design of geomembrane liner systems. The test was conducted using the 2-m x 1-m shaking table on the 9.1 m-radius, 240 g-ton centrifuge at the University of California at Davis Center for Geotechnical Modelling under the U.S. National Science Foundation Network for Earthquake Engineering Simulation Research (NEESR) program. A 0.051 mm specialty geomembrane was used to model the liner system. The landfill foundation was constructed of lightly cemented sand and the waste was modelled using a peat-sand mixture. The side slope membrane was underlain by a thin low density polyethylene membrane lubricated on the top side to maximize the difference between the interface shear strength on the top and bottom of the specialty geomembrane and thus maximize the induced tension for model validation purposes. Model instrumentation included thin film polymer strain gages to monitor geomembrane strains and accelerometers to monitor base excitation and waste mass response. The centrifuge model was subjected to an input design motion intended to simulate the Kobe 0807 motion from the 1994 Hyogo-ken Nanbu earthquake at three progressively increasing peak ground accelerations. The data collected from this test is publically available via the NEESR data warehouse.

4.2. Introduction

Large scale centrifuge testing of a model geomembrane-lined landfill was conducted to validate a numerical model for performance-based design of geomembrane liner systems subject to waste settlement and seismic loading. Current state-of-practice design procedures for geomembranes have proven to be inadequate for determining their performance when subject to waste settlement or seismic loads (Arab et al. 2011). The current state-of-practice for seismic design of geomembranes is based upon Newmark seismic displacement analyses. However, Newmark analyses only provide an index of seismic performance and do not actually evaluate the strains and forces induced in the liner due to seismic loading. Furthermore, analyses conducted in accordance with current seismic design criteria cannot explain the tears that occurred in the liner of the Chiquita Canyon Landfill as a result of the 1994 Northridge earthquake (Kavazanjian, et al. 2013). Forces and strains imposed on side slope geomembranes due to waste settlement are often ignored in practice, though some engineers recognize their potential impact on liner system integrity and employ design details to minimize such loads (Thiel et al. 2014). Therefore, a numerical model for explicitly evaluating the forces and strains in geomembrane liners subject to waste settlement and to seismic loading was developed at Arizona State University (Arab 2011, Kavazanjian et al. 2014). This model includes the ability to account for relative displacement (slip) between the liner and overlying materials during settlement or seismic loading, a particularly important and vexing issue. However, this numerical model lacks validation.

4.3. Centrifuge Model Setup

4.3.1 Centrifuge Modeling Principles

Centrifuge testing enables testing of scaled models of geotechnical systems by amplifying the body stresses within the centrifuge model. As the model is accelerated using the centrifuge, body stresses (e.g., gravity loads) increase in direct proportion to the centrifuge acceleration. Based upon centrifuge scaling laws, prototype length also then scales proportionally to the centrifuge acceleration. However, the shear strength and unit weight of the materials in the model remain the same. Therefore, as centrifugal acceleration increases so does the scale of the model and the body stresses in the scaled model are comparable to the stresses in the field. Some geotechnical centrifuges can also apply earthquake-like horizontal motions to the model simultaneously with the centrifuge acceleration. Scaling laws require that frequency content and horizontal acceleration of the earthquake motion also scale with the centrifuge acceleration. Scaling laws for centrifuge modelling are summarized by Garnier et al. (2007).

4.3.2 Model Configuration

Centrifuge testing of a model of a geomembrane-lined landill was conducted using the 2-m x 1-m shaking table on the 9.1 m-radius, 240 g-tonne centrifuge at the University of California at Davis Center for Geotechnical Modelling under the U.S. National Science Foundation Network for Earthquake Engineering Simulation Research (NEESR) program. A 0.051 mm specialty geomembrane was used to model the liner system. The landfill foundation was constructed of lightly cemented sand and the waste was modelled using a

peat-sand mixture. For model validation purposes, the side slope membrane was underlain by a thin (0.1524 mm) low density polyethylene (LDPE) membrane lubricated on the top side to maximize the difference between the interface shear strength on the top and bottom of the specialty geomembrane and thus maximize the tension induced in the membrane.

The Flexible Shear Beam Container (FSB1) at the University of California at Davis (UCD) centrifuge facility was used as the model container. The container was lined with a LDPE membrane to mitigate the potential for damage to the container due to the cemented sand base. The foundation of the landfill was created using a cemented sand to provide a firm foundation for the geomembrane liner system. Centrifuge scaling laws prevented use of a high density polyethylene (HDPE) liner (the typical material used for landfill geomembrane liners in practice) to model the landfill liner due to thickness issues. In the field, a HDPE geomembrane liner is typically about 2 mm thick. The minimum available thickness of HDPE geomembrane was on the order of 0.5 mm, which would result in a prototype liner thickness of 30 mm at a centrifuge acceleration of 60 g (the proposed maximum acceleration for the model). This prototype thickness was considered not representative of actual landfills and therefore was unacceptable. To account for the scaling up of the geomembrane thickness as the centrifuge acceleration increased, the landfill liner was modeled using a 0.051 mm Nafion^{TM} perfluorosulfonic acid/polytetrafluoroethylene (PFSA) membrane resulting in a scaled prototype thickness of approximately 3 mm at the maximum centrifuge acceleration of 60 g (all prototype dimensions are referenced to the 60 g maximum centrifuge acceleration).

A cross section of the centrifuge model is presented in Figure 4.1. The height of the

landfill side slopes in the model was about 0.3 m on both sides, resulting in a scaled side-slope height of 18 m for the prototype. The waste material was created using a mix of Nevada sand and peat moss proportioned to yield a compressibility similar to that of municipal solid waste. The maximum thickness of the waste was about 0.52 m (prototype height = 31 m). The inclination of the side slope was 2H:1V (Horizontal:Vertical) on the left side of the landfill model and 1H:1V on the right side. Both side slopes in the model had a 76 mm-wide bench (4.6 m prototype dimension) two-thirds of the way up the slope (12 m above the base in the prototype). A 0.1524 mm-thick LDPE membrane was placed on the side slopes beneath the geomembrane and lubricated on the top side to lower the interface strength between the foundation and the bottom of the PFSA geomembrane liner and thereby maximize the tension induced in the liner due to downdrag from settlement of the waste and seismic loading for model validation purposes.

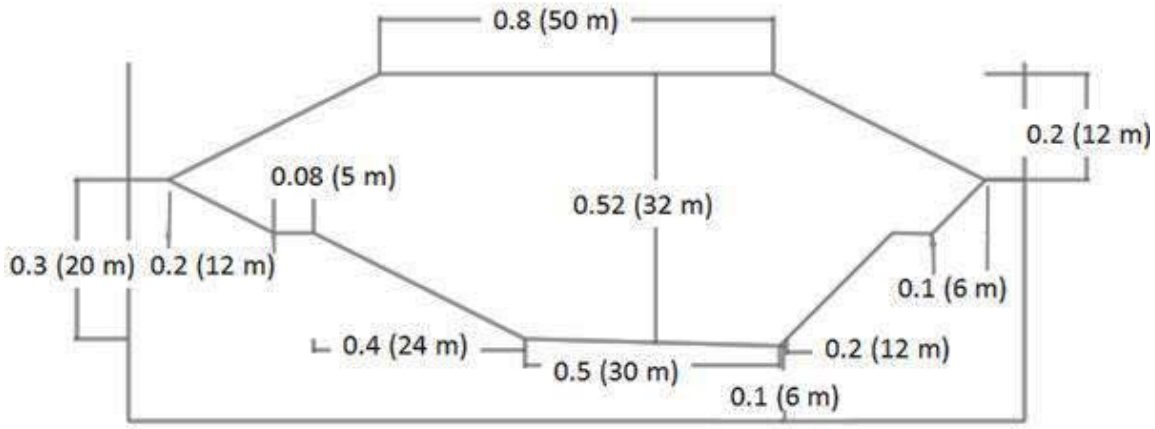

FIG. 4.1. Centrifuge model cross section, prototype dimensions at 60 g in parenthesis (all dimensions in meters)

4.3.3 Cemented Sand Landfill Foundation

The foundation for the landfill model (the portion of the model between the landfill liner and the centrifuge container walls) was constructed using a mixture of Nevada sand and 4% Portland cement (by weight). The Nevada sand and Portland cement were placed in a cement mixer and water was added to provide a water-to-cement ratio of 0.5. The sand, cement, and water were then thoroughly mixed. The initial lifts of the landfill foundation were then constructed by placing sand in the centrifuge container in 25 to 50 mm horizontal lifts and compacting each lift. Compaction was achieved by first tamping the and then placing a wood board on top of the tamped sand-cement mixture and loading the board with a 54 kg mass. The surface of the lift was then scarified prior to placement of the next lift to mitigate the potential for separation of the sand-cement mass between lifts. Two oversized cemented sand mounds were created on each side of the model container by compacting the soil in lifts but without placement of the 54 kg load on top of each lift (to avoid failure of the mounds). Upon completion of the mounds, the cemented sand base and mounds were allowed to set for about 2 hours. Following this 2-hour period, the cemented mounds were shaped into the 2:1 and 1:1 side slopes and benches. A LDPE cover was then placed over the container and the cemented sand foundation for the landfill was allowed to cure for 3 days. Figure 4.2 shows the landfill foundation after shaping of the side slopes.

FIG. 4.2. Cemented sand landfill foundation within the centrifuge model container.

The unit weight of the cemented sand foundation was calculated to be 16.6 kN/m^3 based upon model dimensions and the amount of material employed in model construction. Triaxial compression tests were then conducted on cemented sand samples compacted to the same density. The results of the triaxial compression tests are presented in Figure 4.3. Based upon these test results, the shear strength of the cemented sand can be represented by a friction angle of 29 degrees and a cohesion of 18 kN/m^2.

One-dimensional compression tests were also conducted on the cemented sand model foundation material. This data is needed to subtract the component of the total settlement due to compression of the cement-sand foundation from the total settlement measured at the top of the model. Figure 4.4 shows the results of a one-dimensional compression test conducted on the cemented and material.

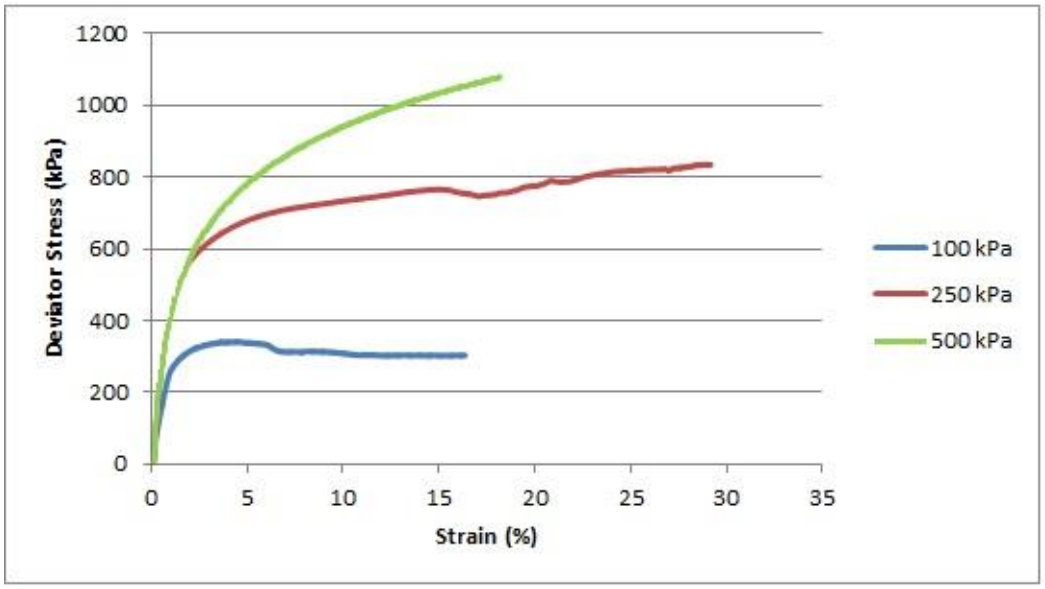

FIG. 4.3. Triaxial compression test results on cemented sand.

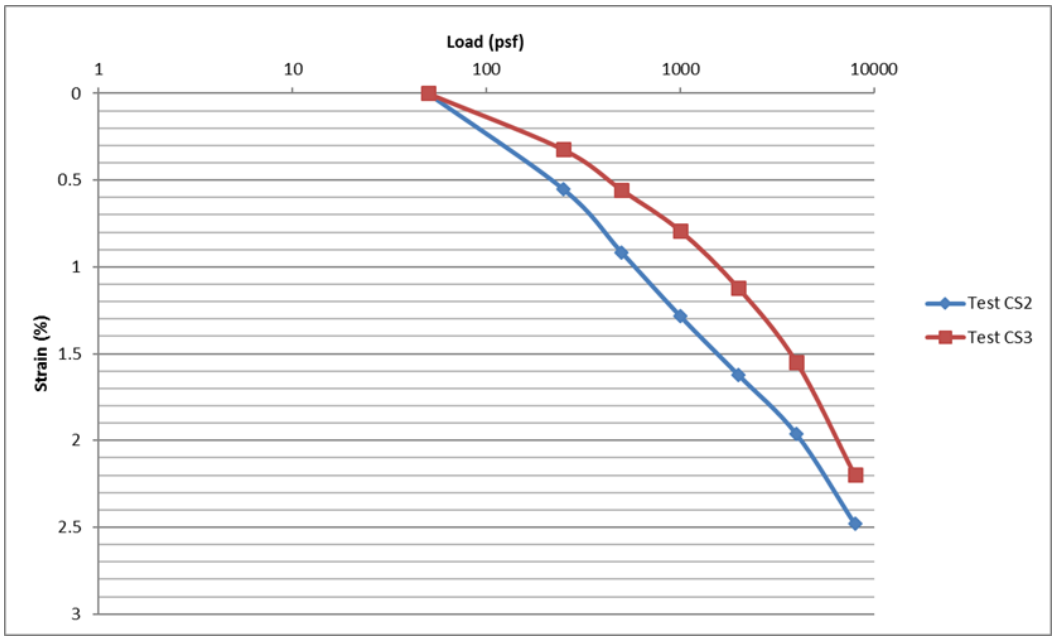

FIG. 4.4. One-dimensional compression tests on cemented sand.

4.3.4 Liner System

The PFSA membrane used to model the landfill liner was the only membrane we found that came in a large enough sheet to cover the foundation of the model and was also thin enough to offset the centrifuge scaling effects. The measured thickness of the PFSA membrane was 0.051 mm, which scaled up to a prototype thickness of about 3.1 mm when the model was accelerated to 60 g. The scaled thickness of 3.1 mm was considered to be close enough to the typical thickness of 1.5 mm to 2 mm for geomembrane liners used in the field for model validation purposes.

The PFSA membrane was placed directly on top of the cemented sand on the base of the landfill and on the benches. On the side slopes, the PFSA membrane was placed on top of a LDPE geomembrane placed on the sand-cement foundation material after lubricating the upper surface of the LDPE geomembrane. The top of the LDPE geomembrane on the side slopes was lubricated to minimize the interface strength on the bottom of the PFSA geomembrane, thereby maximizing tension in the PFSA membrane due to down drag (waste settlement) and seismic loading. The PFSA and LDPE membranes were attached together and anchored at the top of the slope on both sides of the model.

Small scale centrifuge and tilt table tests were conducted to determine the interface strength and stiffness of the PFSA membrane. The interface strength between the PFSA membrane and the sand-peat mixture used to model the waste material was determined to be 26.7° based upon the acceleration at which a block of waste material began to slide in block-on-a-horizontal-plane shaking tests in the small Shaevitz centrifuge at the UC Davis

Center for Geotechnical Modeling. Inverse analyses of the results of the small scale centrifuge tests using the numerical model for performance-based design of geomembranes developed by Arab (2011) yielded frequency-dependent values for the interface stiffness. For a prototype frequency of 1 Hz (a model frequency of 60 Hz at 60 g acceleration), considered to be representative of the input earthquake motion, the back-calculated interface stiffness was approximately 105 MN/m (Wu, 2015). The interface strength between the PFSA membrane and the underlying LDPE was assumed to be negligible where the top of the LDPE membrane was lubricated (i.e., on the side slopes). Where the PFSA membrane was placed directly on the cemented sand foundation material, testing showed that the interface strength between the PFSA membrane and foundation material was greater than the interface strength between the PFSA geomembrane and the waste (which is the only necessary information for model validation).

Tensile tests were conducted on the PFSA membrane to determine its tensile strength and stiffness. The test specimens consisted of a PFSA sheet about 250 mm wide and 75 mm long, satisfying ASTM criteria for wide-width tensile testing of geomembranes (ASTM D4885). The ends of the PFSA sheet were glued to polyurethane bars on both sides. This allowed for gripping of the PFSA sheets for testing. Figure 4.5 shows the clamping system for the PFSA membrane tensile tests and a PFSA specimen within the clamping system fabricated for this purpose. This clamping system was developed to minimize damage to the relatively thin PFSA membrane from clamping. The specimens were strained at a rate of 10%/minute until failure in accordance with ASTM D4885. Figure 4.6 shows the results for two of the wide-width tensile tests on the PFSA membrane.

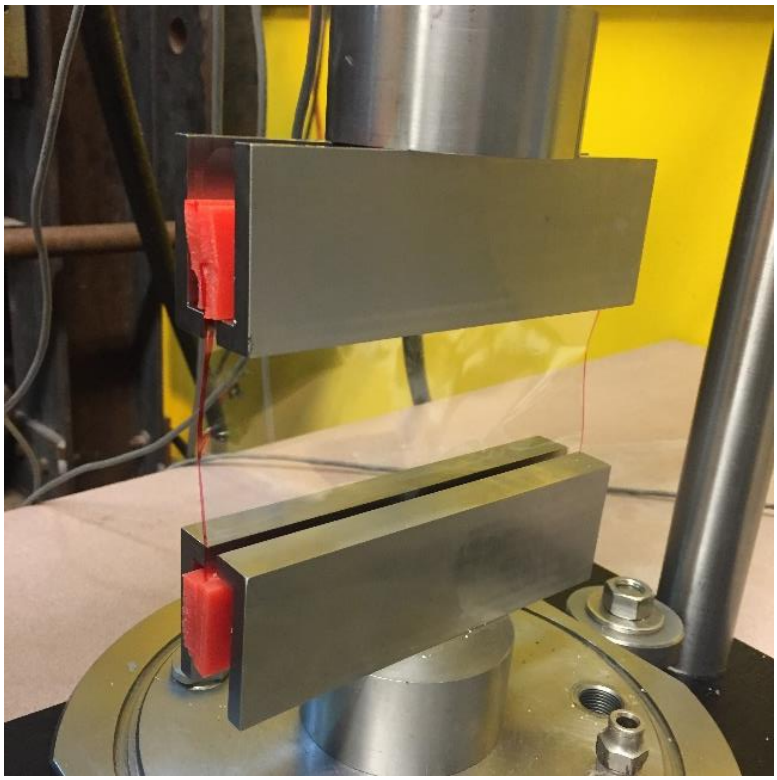

FIG. 4.5. Clamping system for PFSA tensile tests.

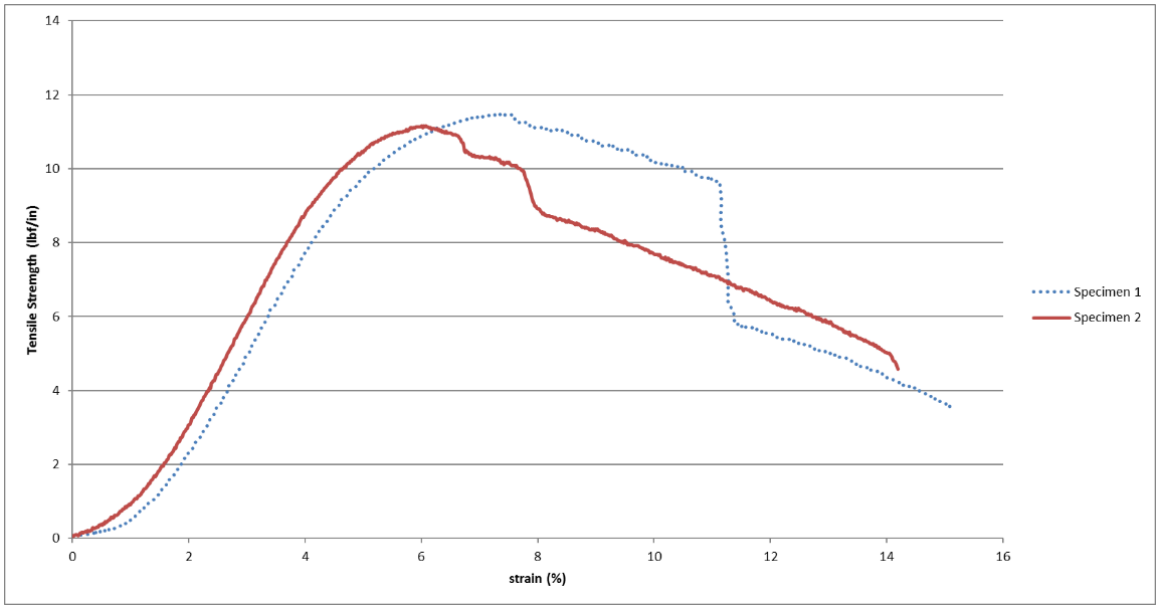

FIG. 4.6. PFSA membrane wide-width tensile test results.

4.3.5 Model Waste Material

A material that exhibited compressibility similar to that representative of municipal solid waste (MSW) was needed to properly capture downdrag effects on the landfill liner. Actual MSW could not be used in the centrifuge tests because of particle size effects, i.e., due to the centrifuge scaling laws. In other words, a twig from common MSW waste would become a log at the prototype scale if actual MSW was used in the model. Therefore, a sand peat mixture, similar to the sand-peat-clay mixture employed by Thusyanthan et al. (2006), was used to model the waste material. Laboratory testing was conducted to determine the appropriate proportions of sand and peat necessary to achieve the desired compressibility.

Based upon numerical modeling of waste settlement due to self-weight consolidation followed by waste decomposition, a compression ratio (C_C) of about 0.10 (virgin compressibility on a volumetric strain vs. log normal stress scale, or the amount of strain over one log cycle) was assumed to be representative of the combined effects of primary compression and long term degradation of MSW (Wu, 2013). Therefore, one-dimensional compression tests were conducted on mixtures with different ratios of sand and peat to obtain a mixture that would provide this level of compressibility. A 1:1 sand:peat mixture (ratio on a mass basis) was initially tested but it quickly became evident that the compressibility of this mixture exceeded the desired compressibility. Figure 4.7 shows one-dimensional compression test results for 3:1 and 4:1 sand:peat mixtures. Based upon the results presented in Figure 4.7, the 3:1 sand:peat mixture was employed in the model. Numerical analysis suggested that this mixture would result in a settlement of

approximately 14% of the initial waste thickness when the model was accelerated to 60 g in the centrifuge. The 3:1 mixture in the one-dimensional compressibility test shown in Figure 4.7 had an initial unit weight of 8.3 kN/m^3. Therefore, this was the target unit weight when the simulated waste material was placed in the model.

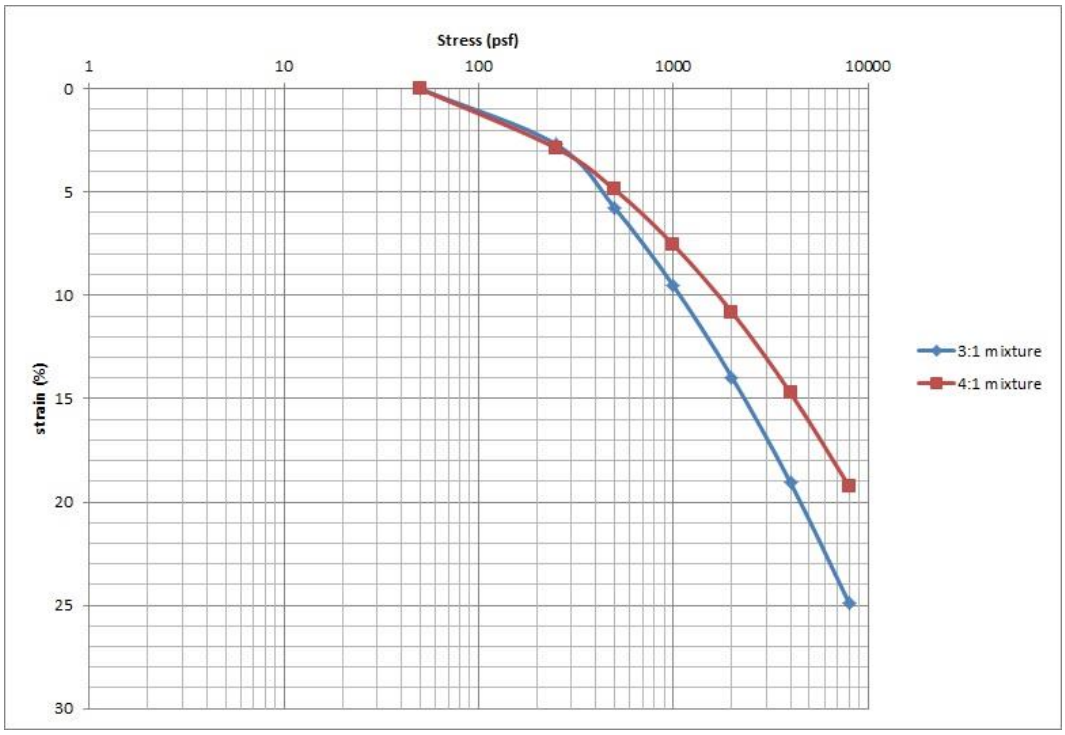

FIG. 4.7. One-dimensional compression test results for the sand:peat mixtures (sand:peat ratio is on a mass basis).

Uniform (sinusoidal) loading cyclic direct simple shear tests (CyDSS) were conducted on the sand peat mixture to obtain equivalent linear modulus and damping values. The CyDSS tests provided resolution down to a shear strain of approximately 0.3 percent. Bender elements were used to evaluate the small strain modulus of the model waste

material. Figure 4.8 shows the shear wave velocity (V_S) measured following one-dimensional consolidation of the sand-peat mixture and the simple shear testing device plotted versus the vertical consolidation stress. Figure 4.9 shows the small strain modulus (G_{max}) values calculated calculate from the V_S values in Figure 4.8 and the corresponding total unit weight values, also plotted versus direct simple shear vertical consolidation stress.

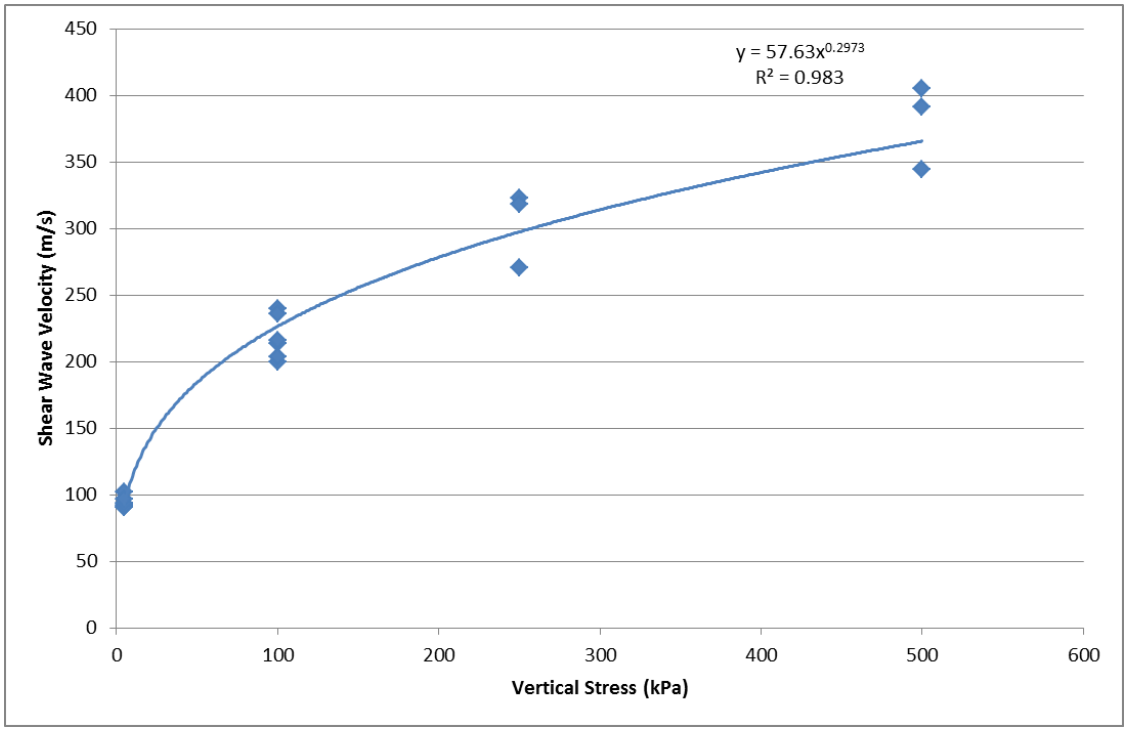

FIG. 4.8. Effective vertical stress in the Direct Simple Shear device vs. shear wave velocity of sand:peat mixture.

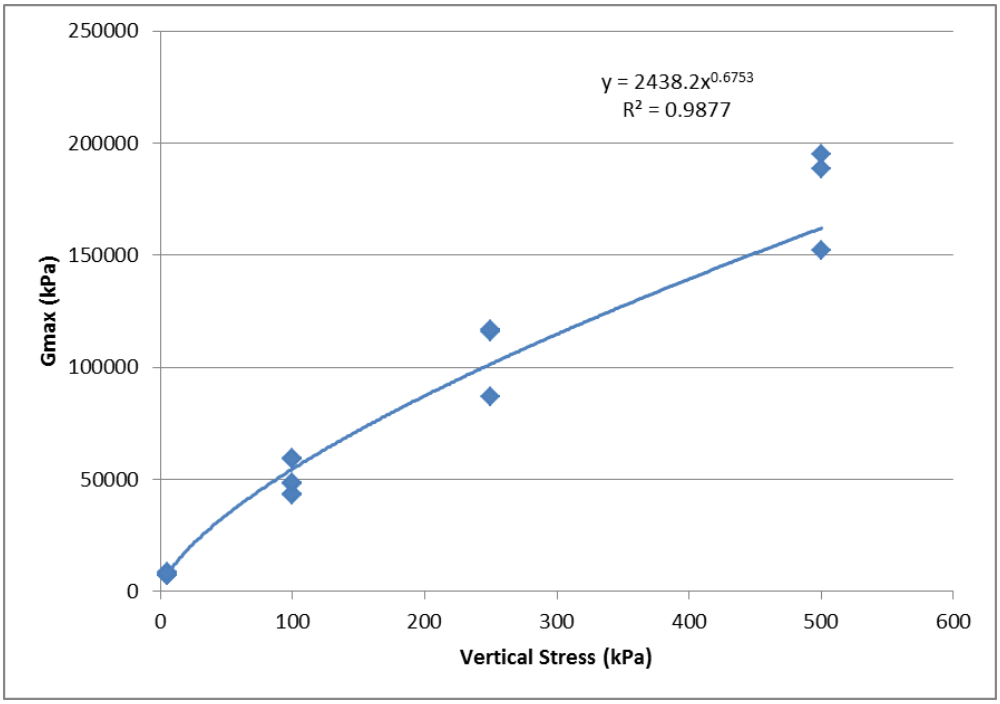

FIG. 4.9. Effective vertical stress in the Direct Simple Shear device vs. G_{max} of sand:peat mixture.

The results of the CyDSS and V_S tests were used to develop the equivalent linear modulus reduction curve for the sand-peat mixture presented in Figure 4.10. The squares in Figure 4.10 represent experimentally-derived equivalent linear modulus reduction values for the sand-peat mixture used to model the waste. The dashed line represents the modulus reduction curve fit to the experimental data based upon the modulus reduction curve for the sand-peat-clay mixture used by Thusyanthan et al. (2006) to model MSW and the upper and lower bound modulus reduction curves presented by Matasovic and Kavazanjian (1998) for solid waste from the OII landfill in southern California. Figure 4.11 provides a similar set of curves and data points for the equivalent linear fraction of critical damping.

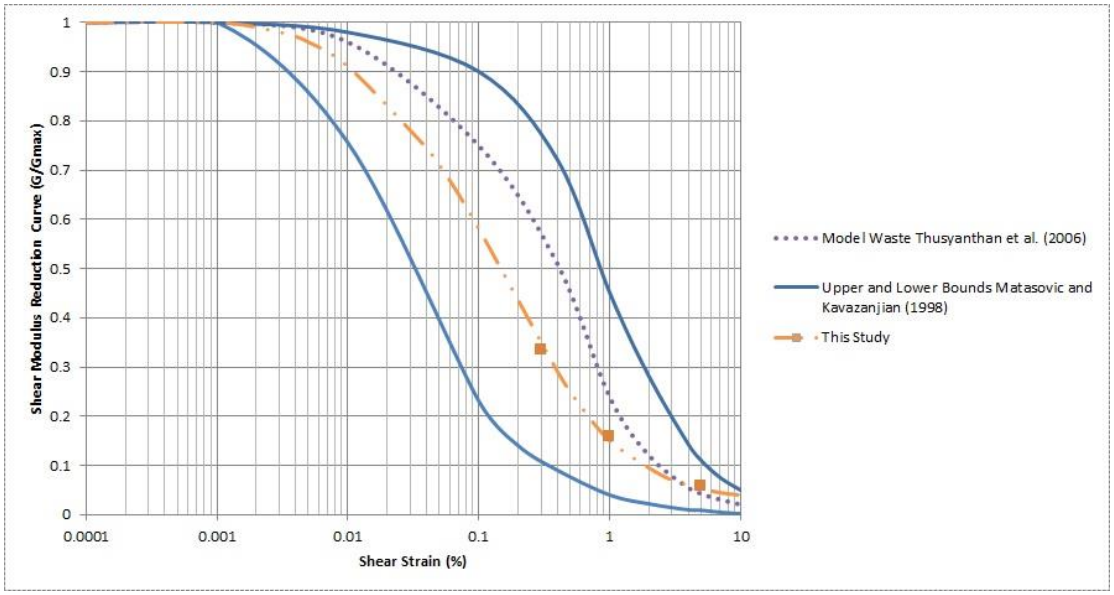

FIG. 4.10. Equivalent linear shear modulus reduction vs. shear strain.

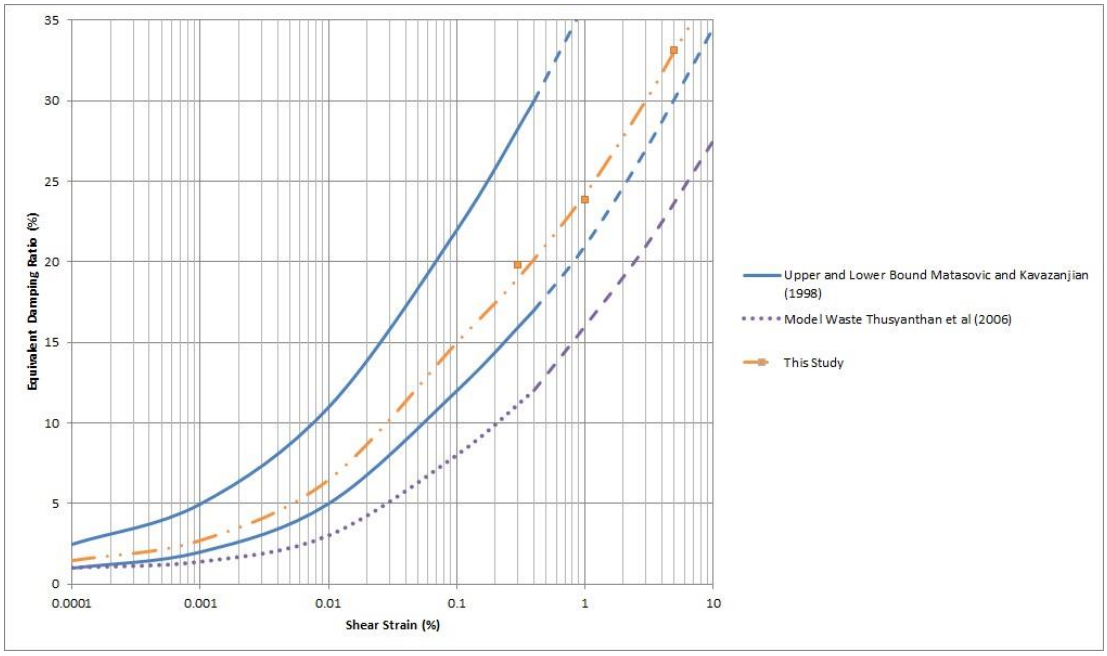

FIG. 4.11. Fraction of critical damping (Damping ratio) vs. shear strain.

4.4 Centrifuge Test Details

4.4.1 Model Sensors

A total of 39 sensors were placed in the centrifuge model to monitor acceleration, displacement, and strain. The sensors consisted of 26 accelerometers, 5 LVDTs, and 8 thin film polymer strain gages. Figure 4.12 shows the sensor locations projected on to the longitudinal cross section of the model. The accelerometers were placed at 13 key points in the model cross section. Two accelerometers (separated longitudinally) were placed at each key point to provide redundancy, i.e. in case one of the accelerometers malfunctioned. The LVDTs were placed at the top of the waste mass to measure waste settlement.

The strain gages were thin film polymer liquid metal-filled strain gages developed by Safaqah and Reimer (2006). The strain gages were glued to the PFSA membrane at 6 locations. Due to the limited number (8) of strain gages that were available, only strain gage locations 3 and 11 in Figure 4.12 (on the benches of the model) had redundant strain gages. These locations were chosen for the redundant strain gages as, based upon numerical analysis conducted by Arab (2011) and Wu (2013), the largest tensile strains expected to be induced on the liner by settlement during centrifuge spin-up and subsequent seismic loading should occur at those locations, i.e., on or near the benches of the landfill.

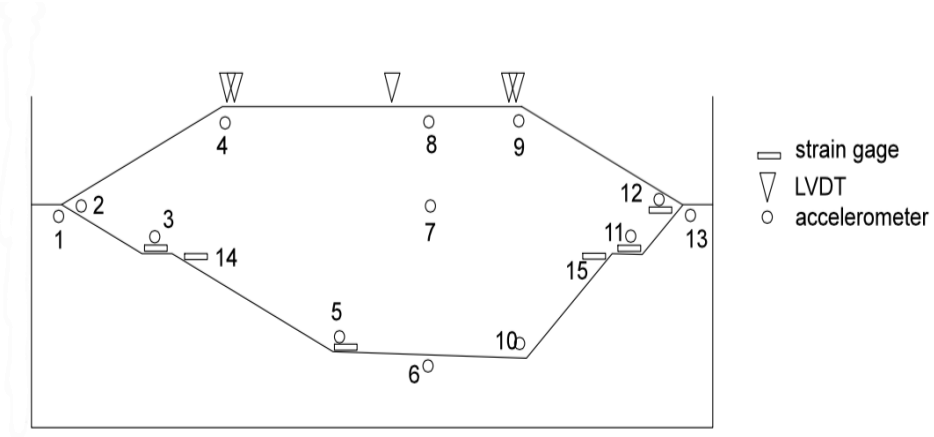

FIG. 4.12. Sensor locations in the centrifuge model.

4.4.2 Testing Sequence

The model was mounted on the centrifuge arm and was spun up to 60 g in three stages. After each stage of loading, the centrifugal acceleration was not increased until the LVDTs showed no more settlement was occurring. Once the waste material stopped settling under the 60 g centrifugal acceleration, the earthquake motion phase of the testing sequence was initiated. A motion modeled after the 1995 Kobe earthquake (Wilson, 1998) was applied to the model three times at successively increasing peak ground accelerations (PGAs). The prototype PGA values for the three motions were 0.05, 0.4, and 0.6 g. Once the final motion was induced, testing was complete and the model was spun down.

4.5 Test Results

4.5.1 Model spin-up

Spinning up the model to 60 g induced approximately 69 mm of settlement (4.2 m on the prototype scale) at the center of the landfill, corresponding to an average vertical strain

in the waste mass of approximately 13.5 % at this location. Settlement of the waste during spin up also induced significant downdrag on the side slope liner system. Table 4.1 shows the cumulative strain on the side slope liner on the benches at location 3 (on the 2:1 slope) and location 11 (on the 1:1 slope) from the three stages of model spin up. Two values are given for each bench as there were two strain gages, separated longitudinally, at those locations for redundancy. The cumulative settlement from the LVDTs at the top of the landfill above these sensor locations and the cumulative settlement from the LVDT at the center of the model are also shown in this table. The settlement on Gage No. 11-1 is an erroneous reading as the LVDT slipped from its seat. Therefore, the settlement of 87.05 mm is not representative of the model settlement.

Table 4.1. Settlement and strains from model spin-up.

Location	1:1 Bench		Center	2:1 Bench	
Gage No.	11-1	11-2	8-1	3-1	3-2
Strain	4.70%	3.30%	N.A.	4.50%	4.57%
Settlement	87.05 mm	66.21 mm	69.17 mm	41.63 mm	69.30 mm

4.5.2 Seismic Loading

Figure 4.13 shows the residual strains induced in the liner on the benches due to seismic loading of the model. The strains on the 1:1 bench are very small, and are actually negative (indicating incremental compression (i.e., a decrease from the tension due to downdrag) at the lower acceleration levels. It is likely that this sensor either malfunctioned

(perhaps due to the load induced by waste settlement) or that the strain on these benches was actually zero and the small negative value is due to noise or the limits of the resolution of the sensors. However, the sensor on the 2:1 bench did show substantial tension induced in the liner by seismic loading, with the induced strain increasing with increasing PGA. Appendix A shows the status of all the sensors in the model at each stage of the centrifuge model test, i.e., whether they were working and malfunctioning. All data collected by these sensors in the centrifuge model test is available in the data warehouse of the Network for Earthquake Engineering Simulation Research (NEESR) at http://nees.org/warehouse.

Figure 4.14 shows the relative displacement between the sand base and the top of the waste material for the 0.05 g motion and the 0.6 g motion. This relative displacement was obtained by double integration of the acceleration time histories from sensors 5 and 6 and then by subtracting the two resulting displacement time histories. Figure 4.14 shows that, while no relative displacement (slip) occurred between the liner and the waste under the 0.05 g motion, there was relative displacement between the waste and the liner under the 0.6 g motion.

Figure 4.15 shows the normalized response spectra for the sand-cement foundation beneath the base of the landfill and at the top of the overlying waste mass at 0.05 and 0.6 g. The normalized response spectra show significant spectral amplification under both the 0.5 g and 0.6 g base motions. The normalized spectra also show an increase in the predominant period of the waste mass response and a decrease in peak spectral amplification of the waste mass under the 0.6 g input motion compared to the 0.05 g motion. This pattern of behavior is characteristic of the effects of non-linear waste mass

behavior and waste-liner interaction on the landfill response. Note that the peak ground acceleration at the top of the landfill also showed similar amplification characteristics, with the input motion being amplified by a factor of 3.7 for the 0.05 g input motion (to .185 g at the top of the landfill) and by a factor of only 1.02 for the 0.6 g input motion (to .613 g at the top of the landfill).

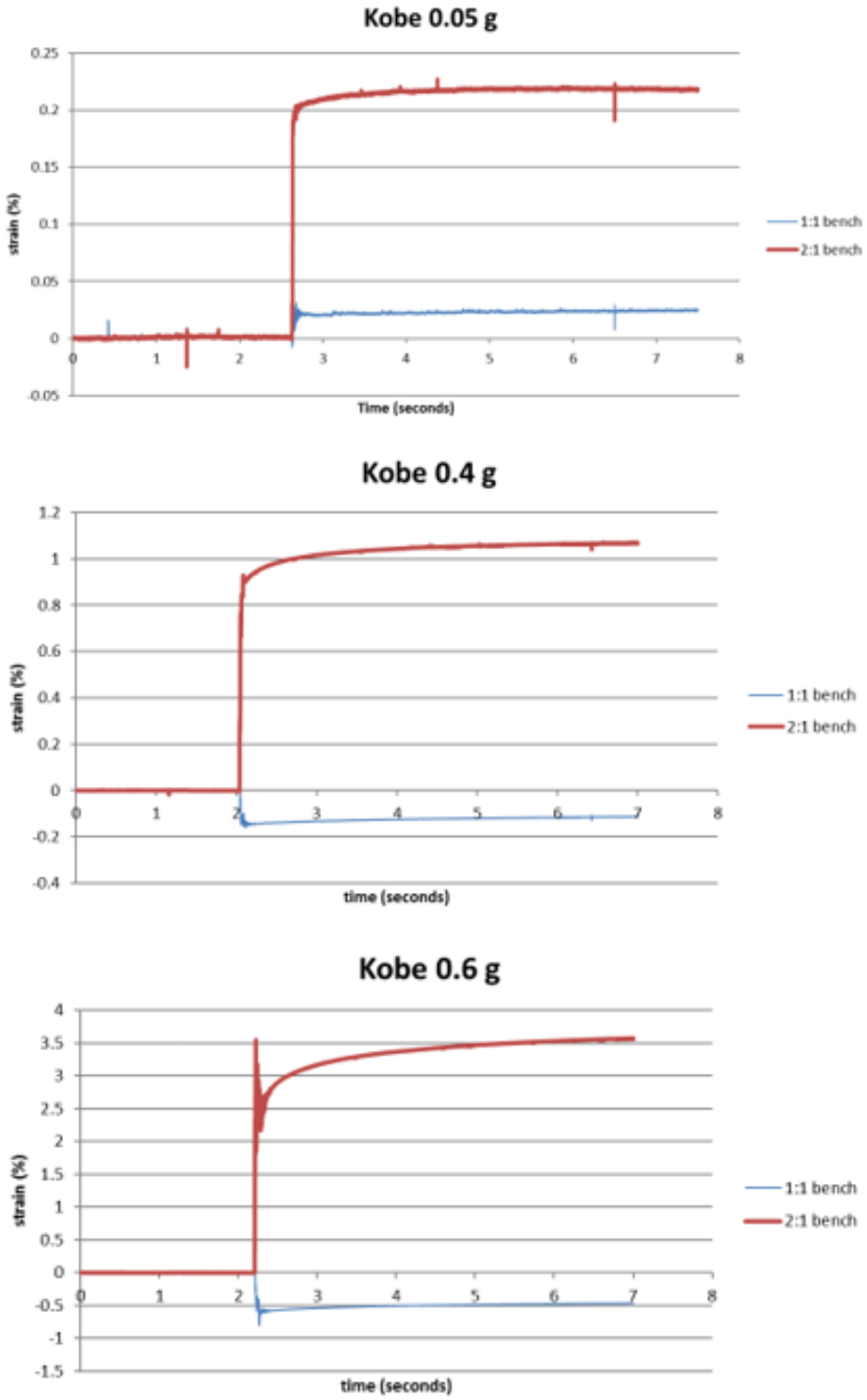

FIG. 4.13. Recorded strain on the side slope benches due to seismic loading.

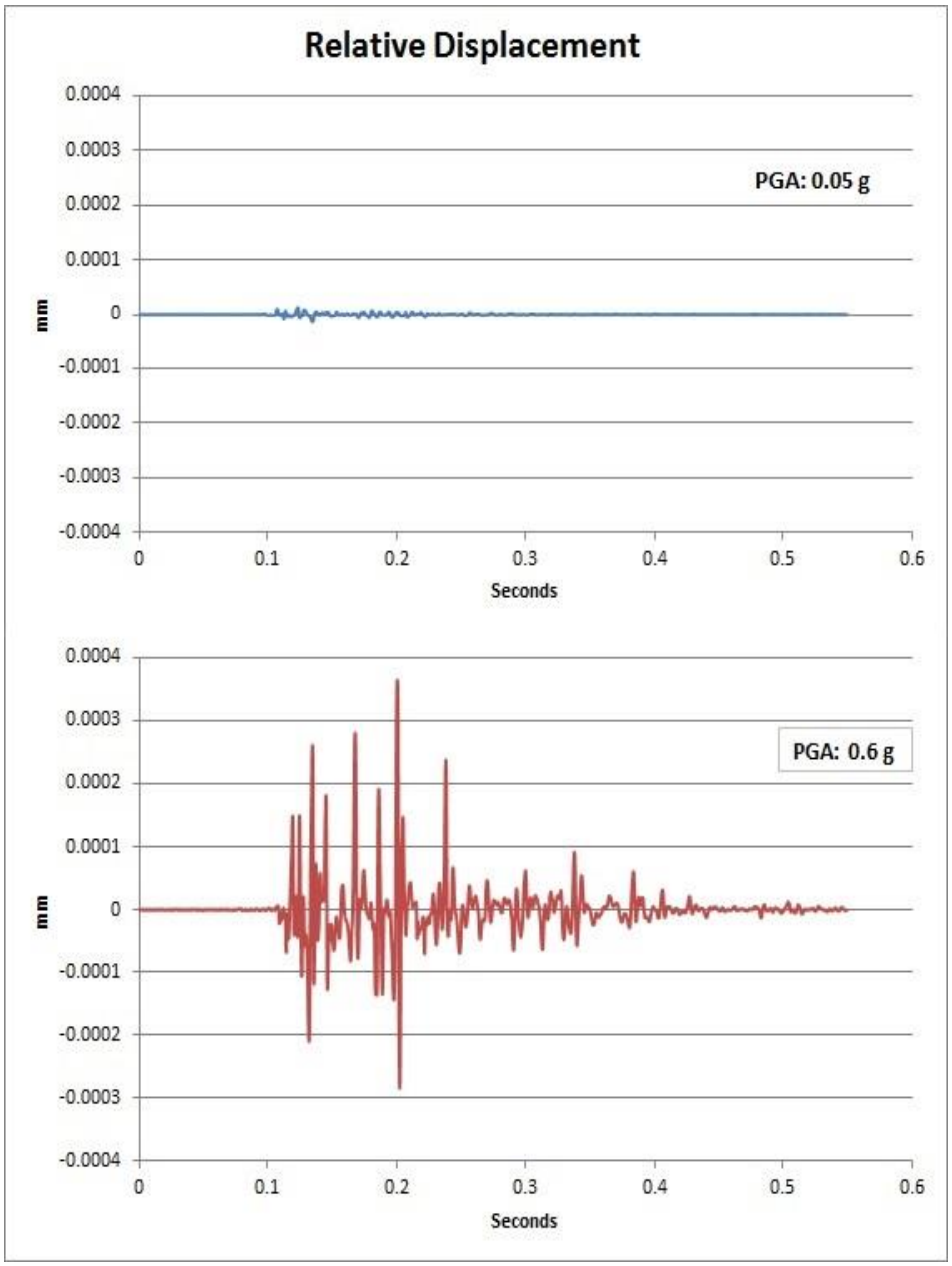

FIG. 4.14. Relative displacement between the foundation and waste at the base of the landfill.

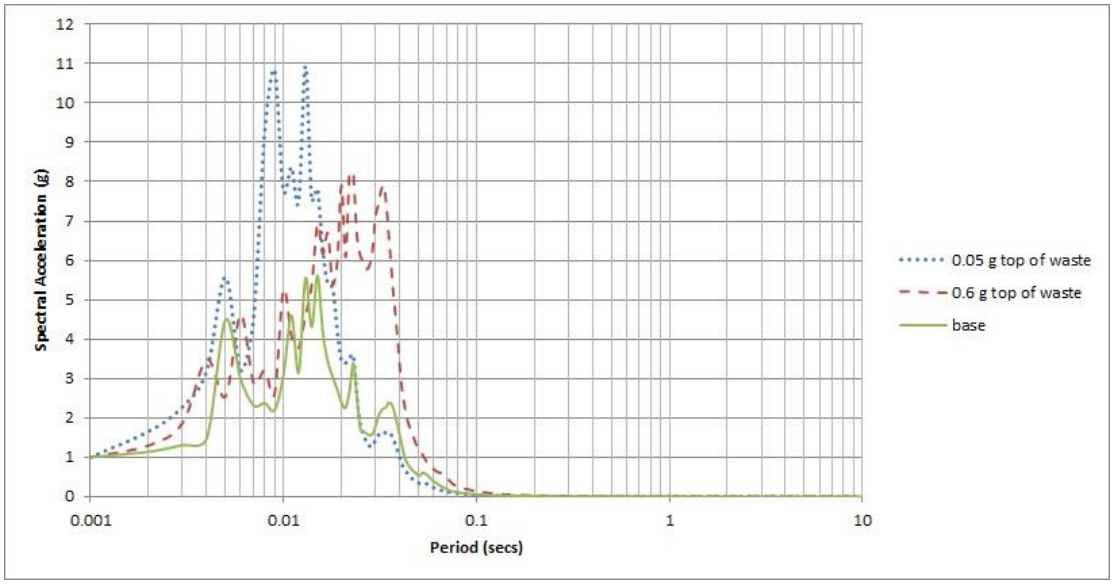

FIG. 4.15. Normalized response spectra at base and top of waste at 0.05 and 0.6 g.

4.5 Summary and Conclusions

A large scale centrifuge test of a model geomembrane-lined landfill was conducted at the UC Davis centrifuge test facility under the United States National Science Foundation (NSF) Network for Earthquake Engineering Simulation Research (NEESR) program. Data collected in this test included liner strains due to downdrag induced by waste settlement during model spin up to a centrifuge acceleration of 60 g, liner strains induced by seismic loading of the model subsequent to spin up to 60 g with input motions of peak horizontal acceleration from 0.05 g to 0.6 g, and acceleration time histories of the model foundation and the waste mass at each of the three peak horizontal acceleration levels. Data from laboratory tests on the materials employed in the centrifuge model supplement the centrifuge test data to provide a data set that can be used to validate numerical models for geomembrane liners subject to waste settlement and seismic loading. All of the data

collected on this project, including the centrifuge test data and supplemental laboratory testing, as well as the results of the numerical validation analyses, has been archived and is publically available via the Network for Earthquake Engineering Simulation (NEES) project warehouse at https://nees.org/warehouse.

Chapter 5

5.0 GEOMEMBRANE SEAM STRAIN CONCENTRATIONS

5.1 Introduction

Strain concentrations have long been recognized as an issue in establishing the allowable tensile strains for geomembrane liners. Despite the fact that the yield strain of a typical HDPE geomembrane subject to a uniaxial tensile load is on the order of 11% to 14%, allowable tensile strains in US practice are typically on the order of 4% and allowable strains in European practice are even less than this. Numerical analyses by Kavazanjian et al. (2013) of the liner tears that were observed in the Chiquita Canyon landfill following to the 1994 Northridge earthquake yielded maximum tensile strains due to the earthquake loading of less than 3 % at the locations of the tears. Kavazanjian et al. (2013) concluded that the tears could only be possible if strain concentrations at seams parallel to the applied tensile load were considered.

In order to explain the tears in the Chiquita Canyon landfill geomembrane observed following the earthquake, Kavazanjian et al. (2013) invoked geomembrane seam strain concentration factors presented in Giroud et al. (1995) and Giroud (2005). Giroud et al. (1995) showed that the bending required for two geomembranes of constant thickness joined at a seam to remain co-planar away from the seam when loaded in tension induced additional (incremental) tensile strains in the vicinity of the seam. Figure 5.1 illustrates the concept of seam strain concentrations due to bending, wherein incremental tensile strains are induced at points A and B at the opposite edges of the seam.

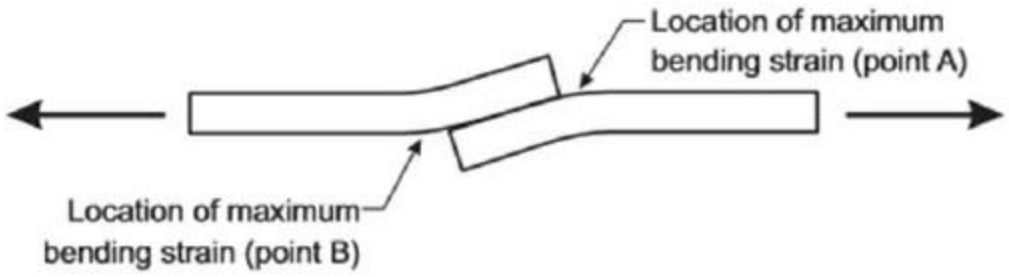

FIG 5.1. Location of incremental bending strains induced adjacent to a seam in a geomembrane loaded in tension (Giroud, 2005).

Figure 5.2 presents the strain concentration factors developed analytically by Giroud et al. (1995) for two different geomembrane thicknesses for a seam width of 30 mm. As illustrated in these figures, the incremental strain adjacent to the seam depends not only upon the seam thickness and seam width, but also on the type of seam (i.e., extrusion versus fusion weld) and the thickness of the seam itself. Giroud et al. (1995) presents equations that can be used to calculate the seam strain concentration factors for any set of values of geomembrane thickness, seam width, seam type, and seam thickness. While these seam strain concentration factors are theoretically sound, no physical testing has been conducted to validate them. Therefore, a testing program was developed at Arizona State University to physically validate the Giroud et al. (1995) strain concentration factors.

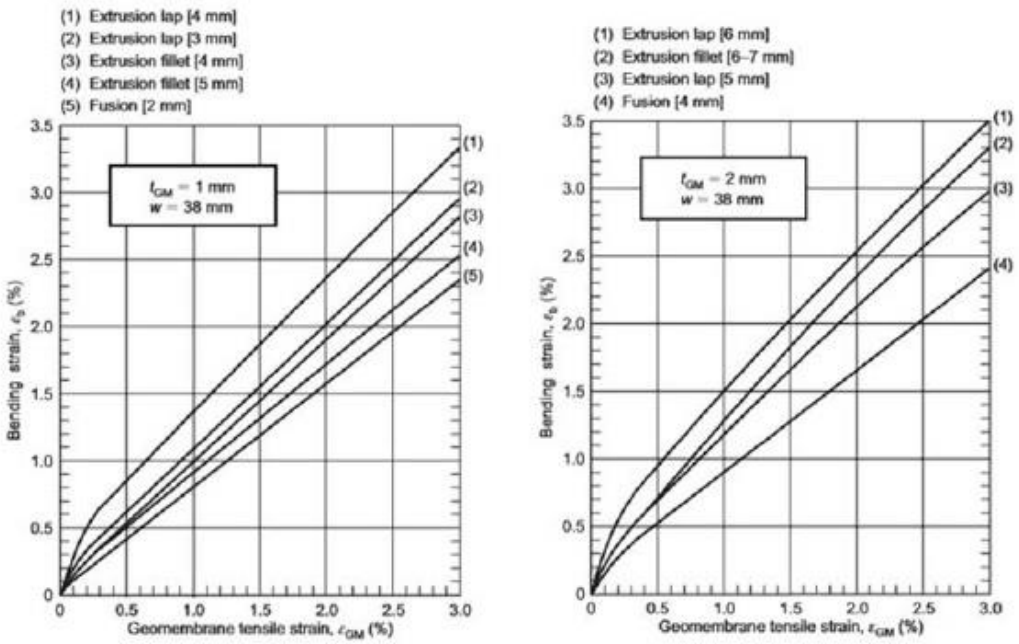

FIG 5.2. Incremental bending strains vs. normal geomembrane tensile strain for different seams in 1 mm (40-mil) and 2 mm (80-mil) geomembranes (Giroud, 2005).

5.2 Geomembrane Samples

5.2.1. Geomembrane Coupons

High density polyethylene (HDPE) geomembrane coupons 1 mm (40 mil) and 2 mm (80 mil) in thickness with extrusion and fusion seams were prepared by a leading geomembrane manufacturer for the seam strain concentration testing program. Each coupon was 135 mm-tall x 150 mm-wide. Two 40 mm-tall HDPE bars were welded on each end of the coupon so they could be clamped between the jaws of a loading frame. The middle section of the coupon (i.e., the section between the bars) was therefore 75 mm-tall by 150 mm-wide, satisfying ASTM requirements for wide-width tensile testing. Figure 5.3 illustrates the configuration of the coupons.

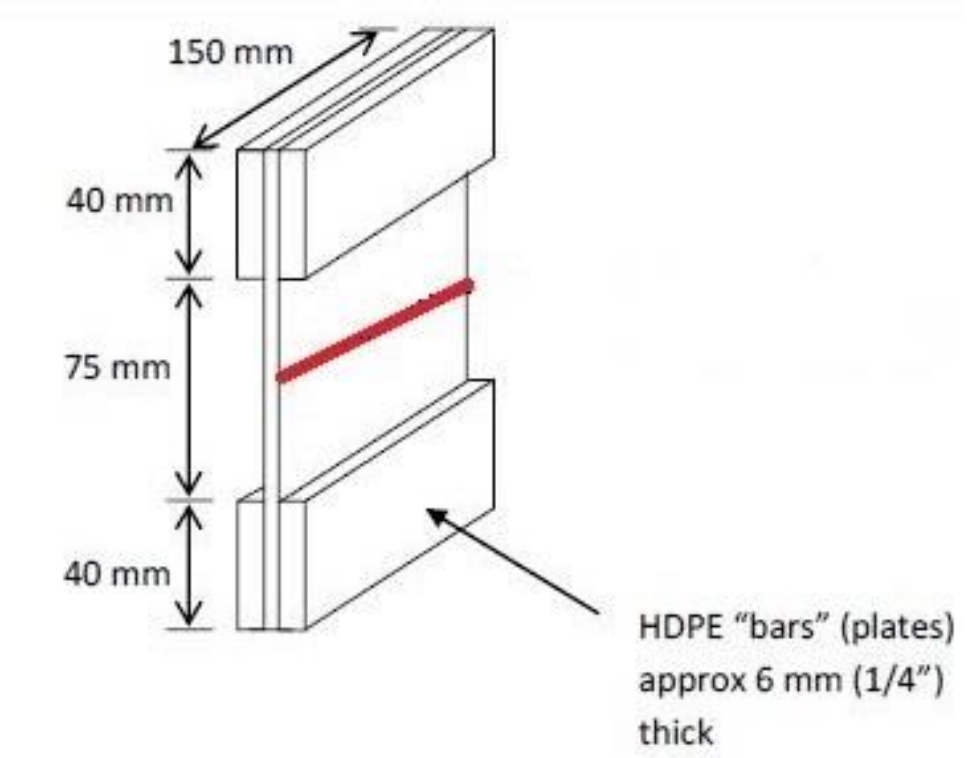

FIG 5.3. Geomembrane coupon diagram with dimensions.

A total of 24 HDPE geomembrane coupons were tested. 12 HDPE geomembrane coupons were 40-mil (1-mm) thick while the other 12 HDPE geomembrane coupons were 80-mil (2-mm) thick. Each 12 coupon group consisted of 4 HDPE geomembrane samples with no seam, 4 HDPE geomembrane extrusion weld seam samples, and 4 HDPE geomembrane fusion weld seam samples.

5.2.2. Geomembrane Coupon Preparation

Because the strain concentrations associated with a geomembrane seam are extremely localized, they cannot be measured using strain gages or other conventional

strain measurement techniques. Therefore, digital image correlation (DIC) was employed to measure the strain field around the seam (and over the entire geomembrane coupon). For a DIC test to be effective, the surface of the coupon has to be prepared in a manner such that distortions of the coupon can be optically detected. A coupon of uniform color or texture, e.g. an entirely black coupon, would not be amenable to DIC. High gloss surfaces can also make DIC ineffective due to reflections from the high intensity lighting used to illuminate the coupon. Therefore, preparation of the samples consisted of first applying a uniform coat of white non-gloss paint on the surface of the coupon. Once the white non-gloss paint was dry, a random pattern of black speckles was applied over the white background and allowed to dry.

The details of the speckle pattern are of upmost importance in acquiring proper results from the DIC test. If a speckle is too large, a data gap is created in the analysis. However, if a speckle is too small the image analysis program may not recognize it. Changes in speckle density can also create gaps in the data. Figure 5.4 shows a HDPE coupon properly prepared for DIC strain measurements.

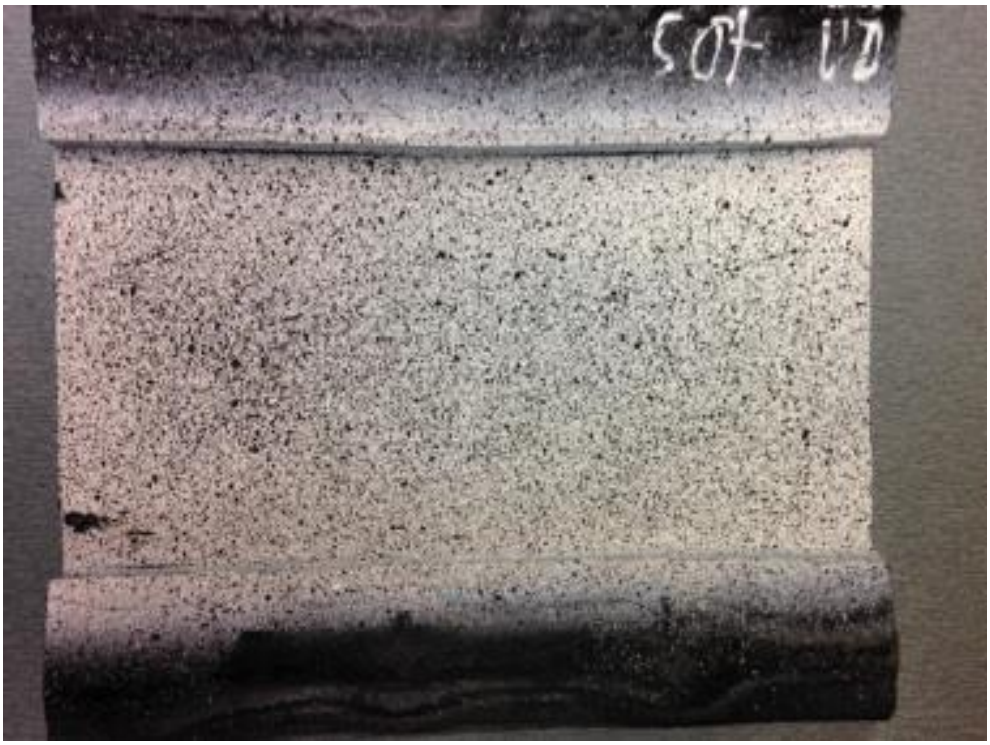

FIG 5.4. HDPE coupon prepared with speckle pattern.

5.3 Testing Apparatus

A triaxial test apparatus was modified to conduct wide-width geomembrane tensile tests according to ASTM D4885 using the geomembrane coupons with the bars attached. The coupon bars slide into grips at each end of the apparatus and a tensile load is applied on the coupon. The clamp system was designed to minimize the potential for strain concentrations along the grip points. Figure 5.5 shows the testing apparatus while figure 5.6 shows a close-up of the clamp system.

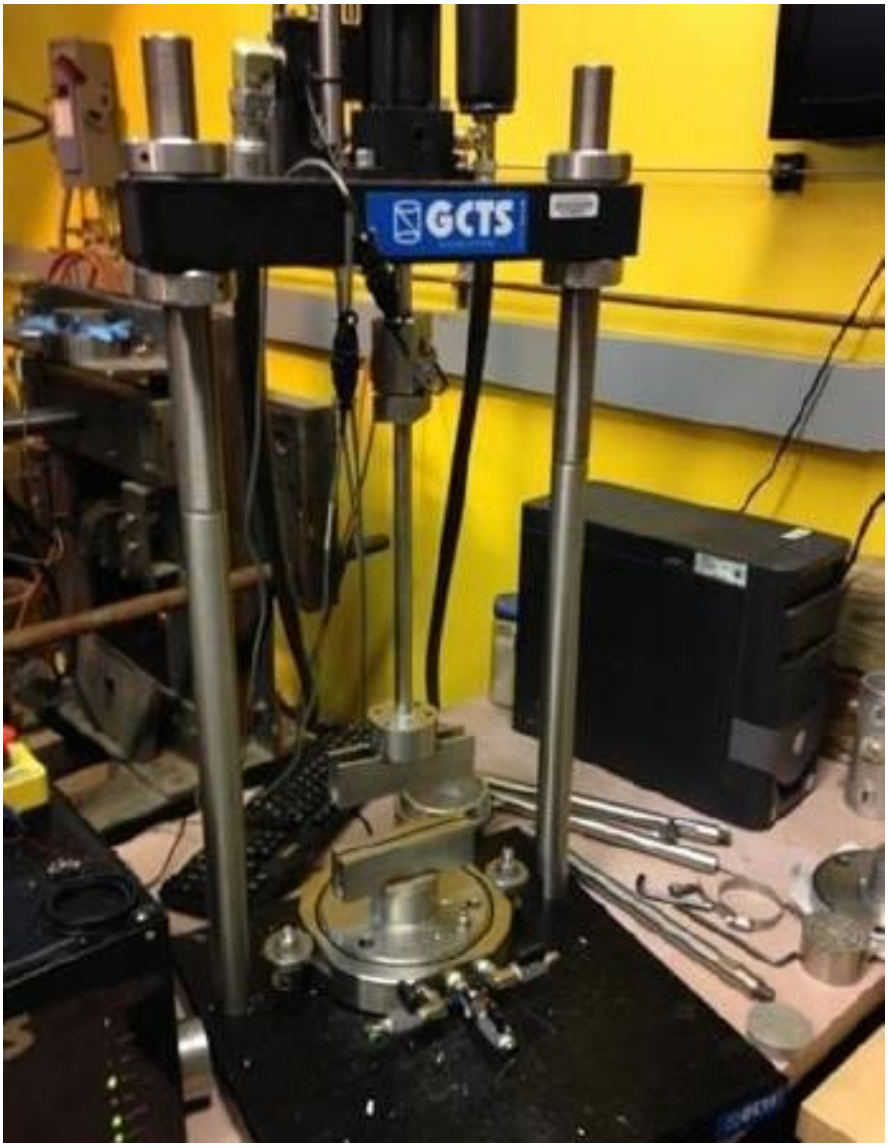

FIG 5.5. Modified triaxial test apparatus for wide-width tensile testing of geomembrane coupons.

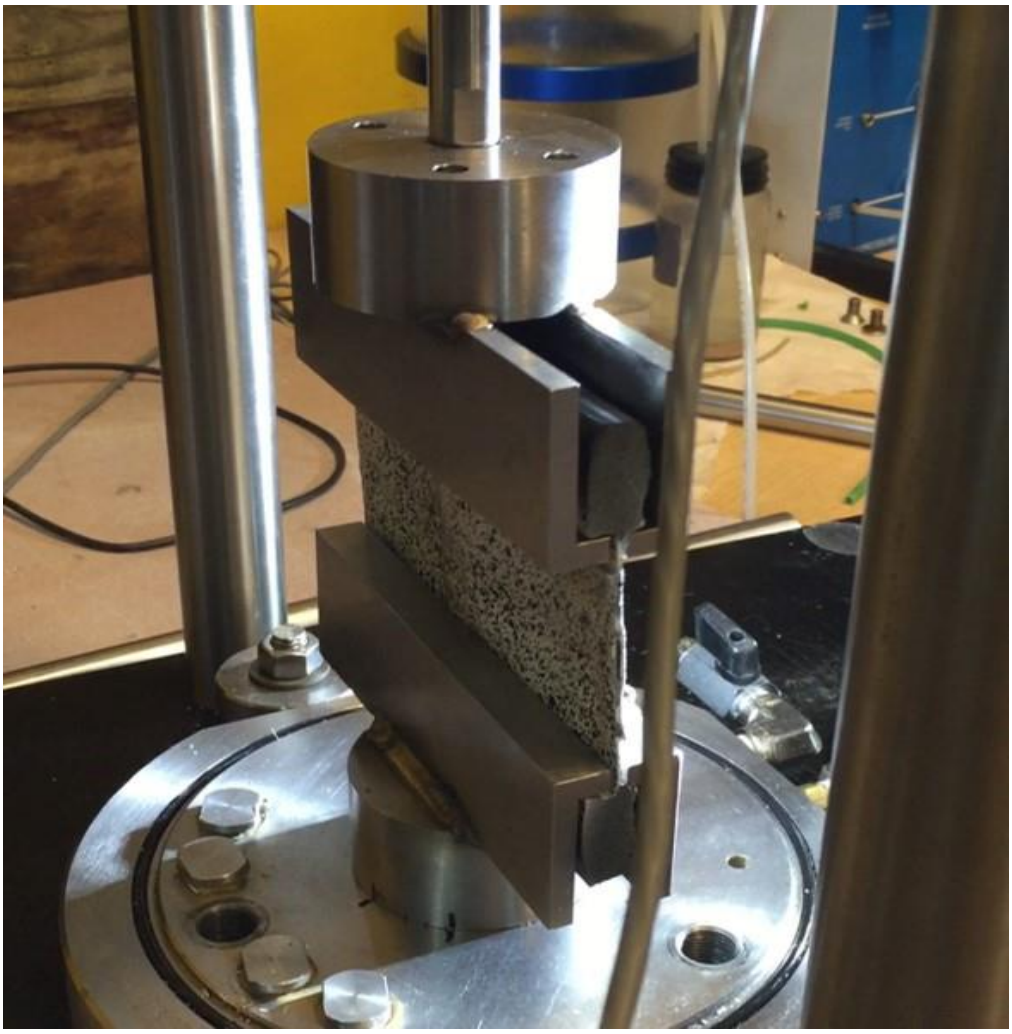

FIG 5.6. Close-up of clamp system with coupon inserted, ready to be tested.

5.4. Test Program

5.4.1. Digital Image Correlation (DIC) Equipment Setup

The DIC equipment includes a tripod which has two LED lights, two high resolution cameras, and a computer that runs the software for image capture. The image capturing software used on this project was VIC Snap. The equipment is setup so the cameras are imaging the sample coupon from different angles but have the same size image

and field of view in the viewfinder. The lights have to be adjusted to provide approximately the same amount of exposure for each camera. Furthermore, ideally, the lighting should be uniform across the surface that is being analyzed. Differences in light coverage across the coupon surface should be minimized and mirrored in the two images captured by the cameras. Any necessary exposure adjustments should be done by adjusting the lighting, with slight adjustments on the cameras themselves being the last resort. Once proper exposure is achieved, the camera focus was adjusted to obtain clear, crisp images from both cameras. Figure 5.7 shows the DIC equipment setup. After proper exposure and focus is obtained on both camera images, the DIC equipment must be calibrated.

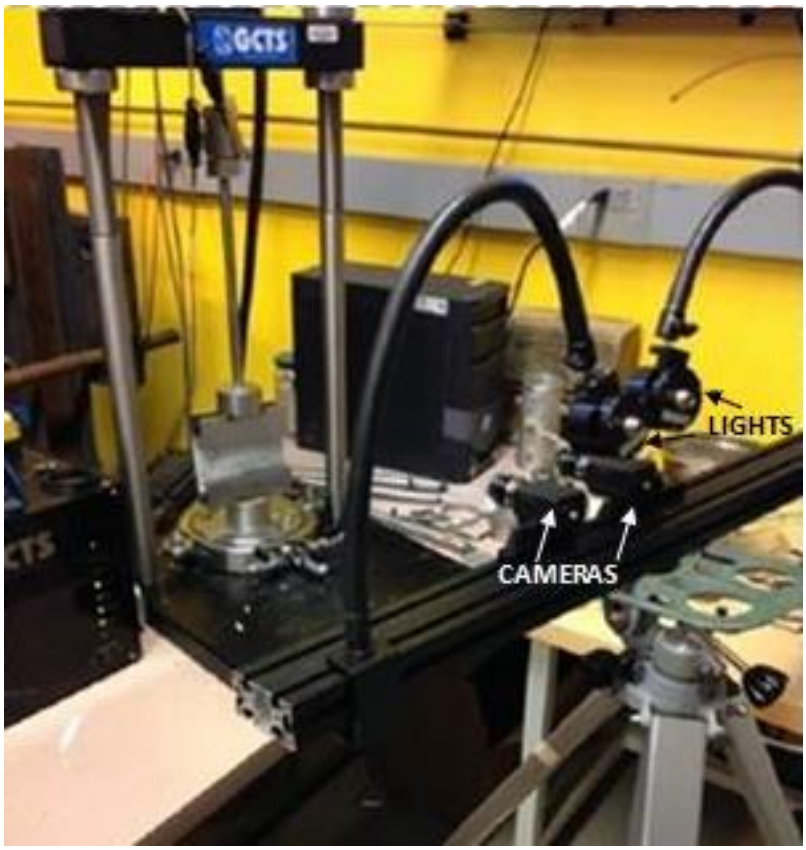

FIG 5.7. Complete test setup with DIC and triaxial equipment.

5.4.2. DIC Calibration

The DIC equipment must be calibrated after setup. Calibration consists of removing the HDPE coupon from the triaxial clamps and inserting a calibration plate of known dimensions. The calibration plate, supplied by Correlated Solutions, Inc., is then rotated along its three axes by hand. While the calibration plate is being rotated, a series of photos are taken with the cameras. These photos are then imported into the VIC3D and used to calibrate the test setup. The calibration process compares the differences between each image that is imported into VIC3D. A score is given at the end of the calibration. This score indicates if the test setup is adequate. If the error is below 1%, the calibration is satisfactory and testing may be conducted. If not, calibration images may be retaken and another calibration in VIC3D may be conducted as sometimes the calibration is not satisfactory due to human error. If the calibration still yields unsatisfactory results the equipment setup must be re-aligned. Figure 5.8 shows an image of the calibration plate.

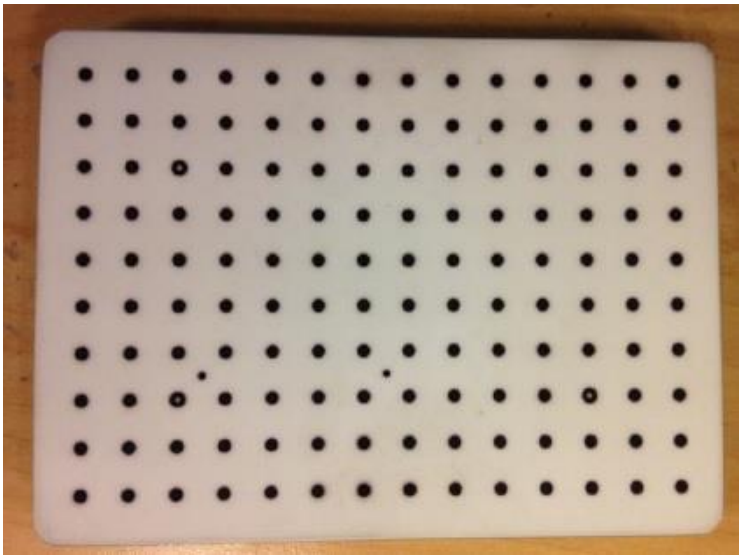

FIG 5.8. Calibration plate supplied by Correlated Solutions, Inc.

5.4.3. Tensile Test Apparatus Setup

The geomembrane coupon was slid into place between the jaws of the testing apparatus. Once the coupon was in place, a seating load was applied to firmly seat the coupon on the clamps. Once the coupon was seated, the sample was deformed in tension a strain rate of 10% per minute in accordance with the ASTM standard for wide-width tensile testing of geosynthetics.

5.5. Tensile Testing

The tensile tests were typically conducted to about 14-16% strain, at which point geomembrane had yielded. Each coupon was assigned a unique identifier that consisted of three components: coupon thickness, seam type, and a letter at the end to differentiate between coupons of the same thickness and seam type. Extrusion fillet seams were designated S1 while dual hot wedge (fusion) seams were designated S2. Therefore, 80S2B would designate an 80 mil- (2 mm-) thick dual hot wedge seam coupon labeled B.

5.6 Analysis

The strain field across each sample was computed using VIC3D. The average tensile strain over the entire coupon between the grips and the maximum strain and the average strain in the vicinity of the seam were calculated at three times during each test. These strains were typically calculated once at an average strain less than 1%, once at an average strain at around 1%, and once at an average strain between 1% and 4%. The

average and maximum strains adjacent to the seams were compared to values predicted using the Giroud et al. (1995) strain concentration factors.

5.6.1. VIC 3D Analysis

VIC 3D calculates the strain field based upon differentiation of the displacement field of the coupon determined by comparison of two images taken at different times. Therefore, a reference image for the unstrained state of the coupon is required from which all DIC analysis is based. In this testing program, the reference image was taken after the seating load was applied to the geomembrane coupons. Using the reference image as the baseline, VIC 3D computes a deformation and strain field over the area of interest based upon the relative movement of the speckles.

Figure 5.9 shows the results of VIC3D analysis for a non-seamed coupon. While the average strain over the coupon was approximately 6% in this image, the coupon exhibits strains between 4% to 8%, with the largest strain at the center of the coupon. This behavior was typical for non-seamed coupons at average strains larger than 3% and is believed due to gentle waves and other non-uniformities in the geomembrane coupons. At strains of less than 3%, the strain field was relatively uniform over the area between the grips of the testing apparatus, although some minor strain concentrations were often observed near the clamps, likely due to non-uniformity of the bars welded to the ends of the coupon for gripping purposes.

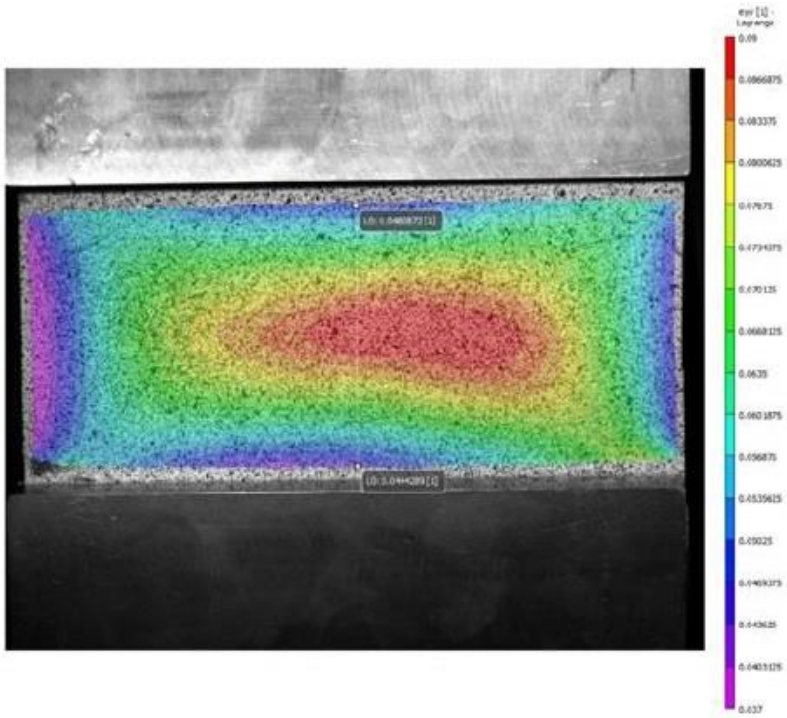

FIG 5.9. 80-mil non-seamed sample at 6.1% average strain (80PA).

Figure 5.10 shows the computed strain field for an 80-mil extrusion fillet seam coupon at an average strain over the mid-section of the coupon of 0.36%. The strain concentration adjacent to the seam is clearly visible as the yellow and red band that spreads longitudinally across the coupon, with an average strain of 0.59% and a maximum strain of 2.8% along this line. Application of the Giroud et al. (1995) strain concentration factors at this stage of the test resulted in a strain adjacent to the seam of 0.89%, relatively close to the average strain measured experimentally but significantly less than the maximum measured value. The discrepancy between the average strain, the strain predicted using the Giroud et al. (1995) strain concentration factors, and the measured maximum values

continued to increase as the global average strain increased, sometimes with the maximum strain reaching 4 times the magnitude of the average strain.

Figure 5.11 shows an example strain field for an 80-mil dual hot wedge fusion seam coupon with an average strain of 2.7%. Again, it can be seen that there is a clear strain concentration adjacent to the seam. In this case, the measured average strain adjacent to the seam was 5.1% and the maximum strain adjacent to the seam was 6.3%. Application of the Giroud et al. (1995) strain concentration factors at this stage of the test resulted in a strain adjacent to the seam of 4.91%, once again approximately equal to the average strain measured experimentally but significantly less than the maximum measured value.

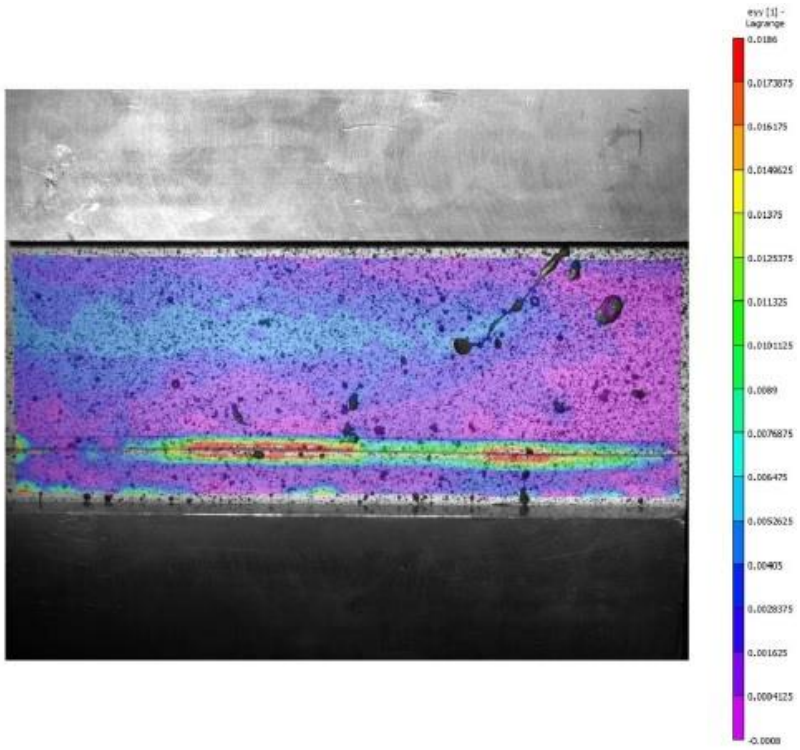

FIG 5.10. 80-mil extrusion fillet coupon at 0.36% average strain (80S1C).

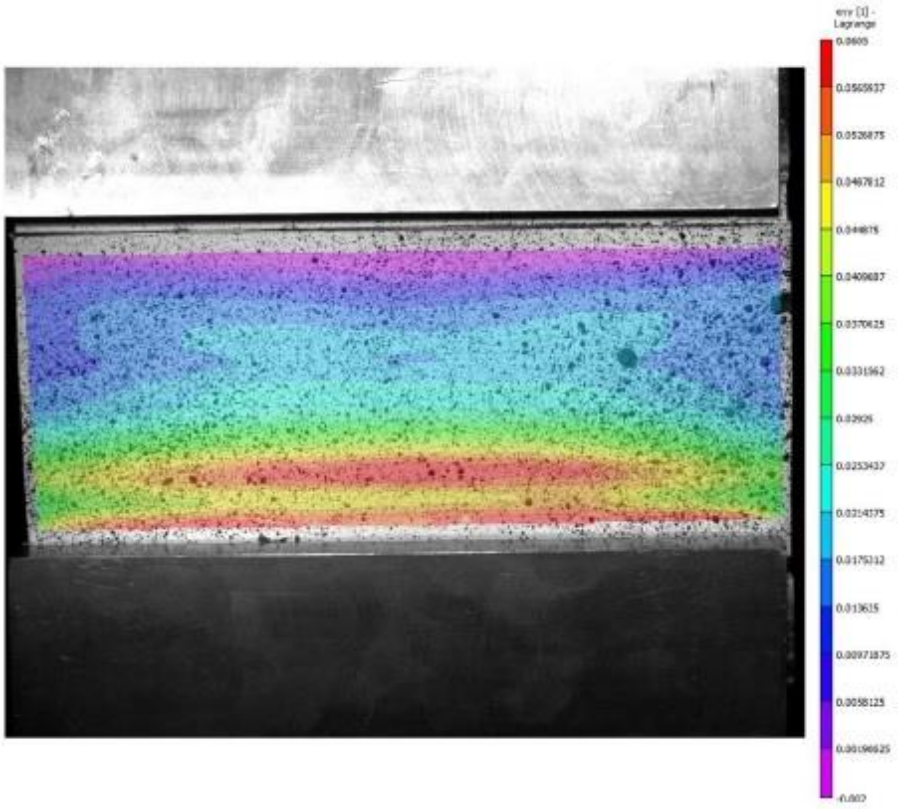

FIG 5.11. 80-mil dual hot wedge seam coupon at 2.7% average strain (80S2A).

5.7 Summary of Results

Table 5.1 summarizes the results of the tests conducted on seamed HDPE coupons for evaluating strain concentrations. The variable ε_{sample} is the global average strain of the HDPE coupon. The maximum strain adjacent to the seam is ε_{max}, while $\varepsilon_{average}$ refers to the average value of the strain in the geomembrane adjacent to the seam. The variable ε_{Giroud} refers to the theoretical incremental bending strain found using the curves in Figure 5.2. The curve number in Table 5.1 refers to the curve from figure 5.2 used to evaluate the Giroud seam strain concentration factor.

Table 5.1. Summary of seamed geomembrane tensile test results.

Sample	Curve	Thickness (mm)	ε_{sample} (%)	ε_{Giroud} (%)	$\varepsilon_{Experimental}$ (%)	
					Max	Average
40S1C	3	4.12	0.1	0.26	0.525	0.034
	3		0.9	1.78	4.79	1.38
	3		2.78	5.45	9.5	7.44
80S1C	2	6.85	0.36	0.89	2.8	0.59
	2		1.45	3.26	5.0	1.10
	2		2.89	6.13	11.6	5.59
40S2B	5	2.15	0.49	0.89	1.3	0.386
	5		1.83	3.24	5.6	2.57
	5		3.5	6.22	11.4	5.48
40S2C	5	2.10	0.378	0.698	2.76	1.75
	5		1.85	3.32	6.51	4.53
	5		3.61	6.38	10.87	8.88
80S2A	4	4.02	0.34	0.87	1.0	0.861
	4		1.36	2.56	3.7	2.80
	4		2.7	4.91	6.3	5.10
80S2B	4	4.26	0.36	0.78	1.21	0.76
	4		1.3	2.42	3.69	3.06
	4		2.83	5.13	9.22	6.52

Figures 5.12 to 5.17 are graphical representations of the results in Table 5.1, comparing four strain values, the average coupon strain, the strain based upon the Giroud strain concentration factors, the average strain in the seam vicinity from DIC, and the maximum strain in the seam vicinity from DIC, for each set of coupons (40 mil and 80 mil geomembrane thicknesses, extrusion and fusion welds).

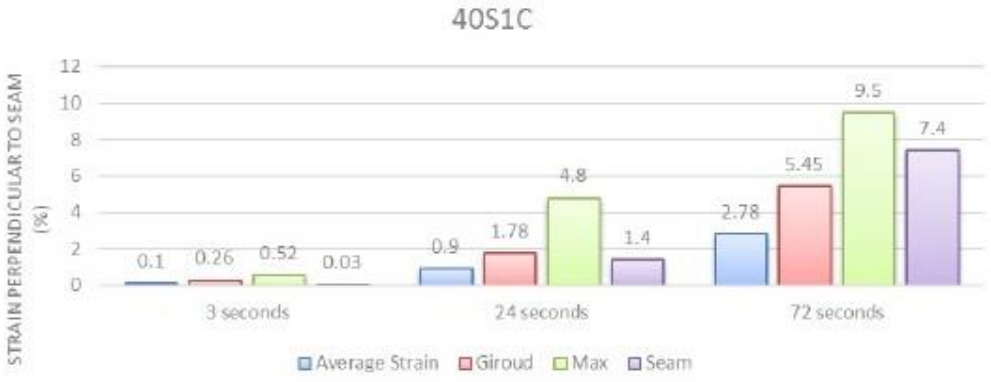

FIG 5.11. 40-mil extrusion fillet seam strains (40S1C).

FIG 5.12. 80-mil extrusion fillet seam strains (80S1C).

FIG 5.13. 40-mil dual hot wedge seam strains (40S2B).

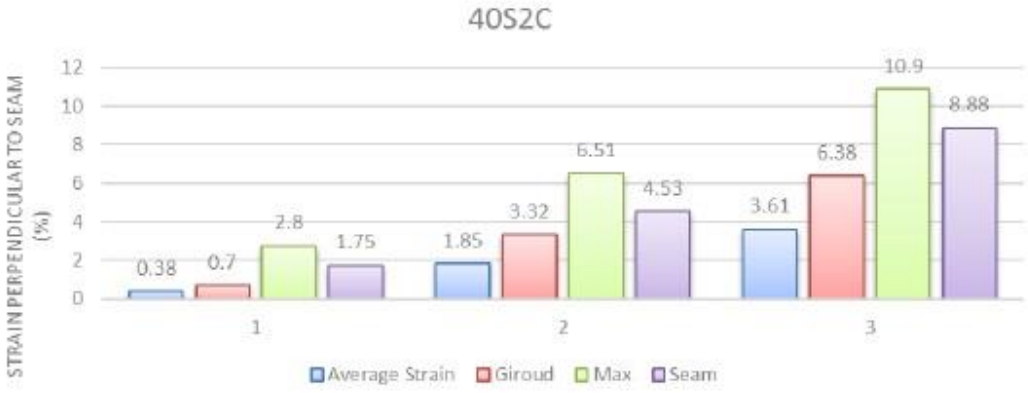

FIG 5.14. 40-mil extrusion fillet seam strains (40S2C).

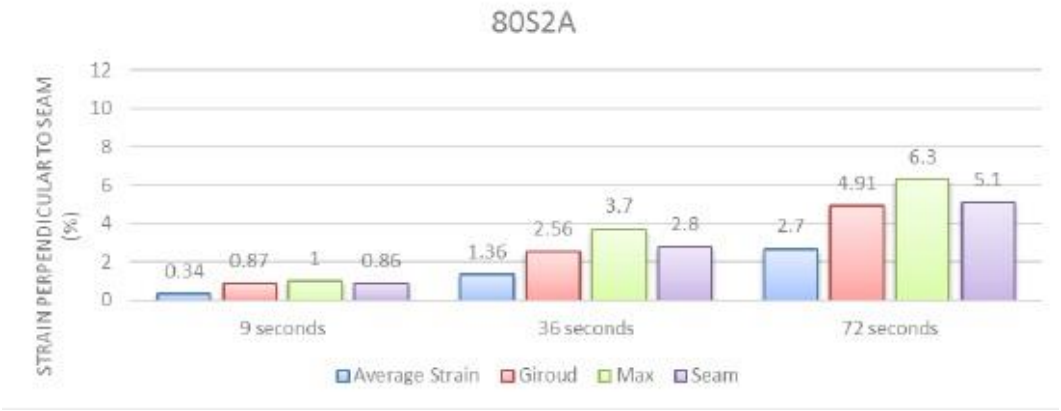

FIG 5.15. 80-mil extrusion fillet seam strains (80S2A).

FIG 5.16. 80-mil dual hot wedge seam strains (80S2B).

The results presented above clearly demonstrate the phenomenon of strain concentrations adjacent to the seams in the geomembrane that are perpendicular to the applied tensile load. While the Giroud et al. (1995) strain concentration factors do reasonable job in predicting the average values of these strain concentrations, the maximum strain concentrations in the geomembrane coupons is significantly higher than that predicted by Giroud (2005). The error between the experimental maximum strain and the theoretical Giroud strain ranged from 13% up to 75% depending on thickness and seam

type. The average normalized difference between the experimental maximum strain and the theoretical Giroud strain was about 43%. The normalized error between the seam length average strain and the theoretical Giroud strain was only about 7%.

5.8 Conclusion

This chapter describes an experimental evaluation of HDPE seam strain concentrations. The experimental approach consisted of using a modified triaxial-test apparatus to applied a tensile load to HDPE geomembrane coupons with seams in them. Images captured as the coupon was being strained were evaluated using DIC. Strain fields computed using DIC provided the location and magnitude of strain concentrations adjacent to the seams in the HDPE coupons. The experimental results were then compared to the theoretical values for seam strain concentrations developed by Giroud et al. (1995).

The results of the analysis clearly show the existence of strain concentrations adjacent the seams as predicted by Giroud et al. (1995). However, while the average strain concentrations measured experimentally were close to those established using the Giroud et al. (1995) strain concentration factors, the maximum strains adjacent to the seams were significantly greater than predicted using the Giroud et al. (1995) factors. The additional incremental strain seen experimentally is likely due to imperfections and non-uniformities along the seam. Considering that the seams tested herein were fabricated in a laboratory under controlled conditions, imperfections and non-uniformities in field seams are likely to be even greater than the seams tested herein, resulting in even larger seam strain concentrations. Testing of field seams should be conducted to see if this hypothesis is valid,

as the value of seam strain concentrations has significant implications with respect to allowable tensile strains in geomembranes and construction quality assurance (CQA) practices for collecting seam samples for destructive testing. Strain concentrations due to scratches in the geomembrane (also evaluated by Giroud et al. (1995)) and due to other irregularities on the surface of the geomembrane should also be considered when establishing allowable strains and CQA practices.

Chapter 6

6.0 SUMMARY AND CONCLUSIONS

6.1 Summary

The purpose of this dissertation was to provide physical data necessary to validate a numerical model that evaluates the performance of landfill liners subjected to downdrag due to settlement and to seismic loading. It is one part of a global objective to enable performance based design of geosynthetic liner systems for waste containment, enhancing environmental protection while facilitating more economical construction.

This project included preliminary tests to determine the compressive modulus of HDPE and evaluate the interface shear strength of between the simulated waste material and thin film geomembrane used in a centrifuge model test of a geomembrane lined landfill, laboratory tests to determine the properties of the materials used to construct the centrifuge model, and spin-up and seismic loading of the centrifuge model. Tests to determine the properties of the materials used in the centrifuge model included one-dimensional compression tests of sand-peat mixtures to establish the appropriate proportions for the simulated waste material, cyclic simples shear tests to determine the modulus and damping of the simulated waste materials, triaxial compression tests of the cemented sand mixture used for the foundation of the model, and tensile tests on the thin film membrane used in the centrifuge model. The centrifuge model was spun up to 60 g in three stages and then subjected to three seismic loads of progressively increasing intensity

Settlement of the waste and strains on the liner system due to downdrag and liner strains and acceleration throughout the model due to seismic loading were obtained from the centrifuge model tests. The results of these tests will be used to validate a numerical model that will be a stepping stone to development of performance based design of geosynthetic landfill liners due to waste settlement and seismic loading. To further develop the methodology for performance-based design, strain concentrations adjacent to geomembrane seams were also evaluated. A series of tensile tests were conducted on geomembrane coupons with seams in them. While tensile loading was being applied, digital image correlation (DIC) was employed to obtain the strain fields on the coupons from images captured during the tensile tests. The DIC analysis provided precise strain measurements over very small, localized areas of the geomembrane coupon. The average strains in the vicinity of the seams measured by DIC were relatively close to strains based upon seam strain concentration factors for geomembranes developed by Giroud et al. (1995) and Giroud (2005), but the maximum strains in the vicinity of the seams was significantly greater than those predicted using the Giroud factors.

6.2. Conclusions

In this research, a set of experiments were conducted to experimentally evaluate parameters required for the validation of a performance based design for geosynthetic liners subjected to downdrag and seismic loading. The findings from the experiments conducted for this dissertation include:

- The data set acquired from the large scale centrifuge test and associated laboratory tests can be used to validate the Arab (2011) FLAC^{TM} numerical model for geomembrane liners subject to waste settlement and seismic loading.
- Strain concentrations present along HDPE geomembrane seams loaded in tension are sometimes up to 4 times the magnitude of global average tensile strain.
- The measured seam strain concentrations are much higher than those predicted using the seam strain concentration factors presented by Giroud et al, (1995) and Giroud (2005).
- 1-dimensional compression test results on sand and on composite HDPE/sand specimens to determine the compressive modulus of HDPE were inconclusive

Recommendations for future work with respect to the large scale centrifuge test are as follows:

- Run a second centrifuge model test to substantiate the accuracy of the data acquired
- Use many more strain gages throughout the model to acquire more data on liner strains
- Strengthen the connections of the strain gages to the data acquisition system since they are relatively delicate
- Obtain data through all aspects of testing (spin-up, settlement, seismic loading, etc.)
- Develop a means of measuring seam strains in the centrifuge test and employ a liner with a seam so that seam strain concentrations can be measured

Recommendations for future work for the HDPE tensile tests for evaluation of seam strain concentrations are as follows:

- Experimentally evaluate the differences between the induced strain concentrations and the Giroud strain concentration factors
- Acquire samples from actual landfill sites to evaluate strain concentrations on actual seams from the field with the associated imperfections

Recommendations for future work to determine the compression modulus of HDPE are as follows:

- Additional testing is need to experimentally evaluate the compressive modulus of HDPE
- A more compressible soil than Ottawa 20/30 sand at a high relative density should be used to accentuate the difference in compressibility between the soil and the HDPE.

6.3. Acknowledgment

The work described herein was funded by the United States National Science Foundation (NSF) Geomechanics and Geotechnical Hazards program of the Civil, Mechanical, and Manufacturing Innovation Division (CMMI) under the Network for Earthquake Engineering Simulation Research program under Grant # CMMI 1208026, "NEESR: Performance-based Seismic Design of Geomembrane Liner Systems for Waste Containment. The author is grateful for this support. Any opinions or positions expressed in this paper are the opinions and positions of the authors only, and do not reflect any opinions or positions of the NSF.

The author would also like to acknowledge the staff at the University of California at Davis centrifuge facility, especially Chad Justice, Anatoly Ganchenko, and Dr. Dan Wilson, for their help in executing the centrifuge testing program. The author also acknowledges the assistance of Dr. Mike Reimer from the University of California at Berkeley for providing the polymer strain gages and training on calibration of the sensors, of Jake Andresen, Sean O'Donnell, and Xuan Wu, graduate students at Arizona State University, for their helping with building and testing the centrifuge model, of Jake Andresen with the geomembrane seam concentration testing, and of Peter Goguen, ASU Geotechnical Laboratory Director, with multiple aspects of the testing program.

REFERENCES

Arab, M.G. (2011). The Integrity of Geosynthetic Elements of Waste Containment Barrier Systems Subject to Seismic Loading. PhD thesis. Arizona State University, Tempe, Arizona.

Arab, M.G., Kavazanjian, E., & Matasovic, N. (2011). Seismic Analysis of a Geosynthetic Liner System. In *Proceedings of GeoFrontiers 2011: Advances in Geotechnical Engineering,* ASCE Special Publication 211, pp. 1981-1990.

Augello, A. J., Matasovic, N., Bray, J. D., Kavanzajian, E., & Seed, R. B. (1995). Evaluation of Solid Waste Landfill Performance During the Northridge Earthquake. In *Geotechnical Special Publication.* 54 ed., pp. 17-50.

Augello, A.J., Bray, J. D., Abrahamson, N. A., & Seed, R. B. (1998). Dynamic Properties of Solid Waste Based on Backanalysis of OII Landfill. In *Journal of Geotechnical and Geoenvironmental Engineering*, 124, (3), pp. 211-222.

Bray, J.D., Rathje, E.M., Augello, A.J., & Merry, S.M. (1998). Simplified Seismic Design Procedure for Geosynthetic-Lined, Solid Waste Landfills. In *Geosynthetics International*, Vol. 5, Nos. 1-2, pp. 203-235.

EMCON (1994). Northridge Earthquake Seismic Evaluation, Chiquita Canyon Landfill. EMCON Associates, San Jose, CA, April.

Fowmes, G. J., Dixon, N., Jones, D. R. V., & Cowland, J.W. (2006). Modelling of Lining System Integrity Failure in a Steep Sided Landfill. In *8th International Geosynthetics Conference, 8ICG.*

Fowmes, G. J. (2007). Analysis of Steep Sided Landfill Lining Systems. Eng.D thesis, Department of Civil and Building Engineering, Loughborough University, Loughborough, UK.

Garnier, J., Gaudin, C., Springman, S.M., Culligan, P.J., Goodings, D., Konig, D., Kuttervi, B., Phillips, R., Randolph, M.F.m Thorel, L. (2007). Catalogue of Scaling Laws and Similitude Questions in Geotechnical Centrifuge Modelling. In *International Journal of Physical Modelling in Geotechnics* 3, 01-23.

Giroud, J. P., Soderman, K. L., & Monroe, M. (1993) Mechanical Design of Geomembrane Applications. In *Proceedings*

Giroud, J. P., Tisseau, B., Soderman, K.L., & Beech, J.F. (1995) Analysis of Strain Concentration Next to Geomembrane Seams. In *Geosynthetics International*, Vol. 2, No. 6, pp. 1049-1097.

Giroud, J. P. (2005). Quantification of Geosynthetic Behavior. In *Geosynthetics International,* Special Issue on the Giroud Lectures, 12, No. 1, 2-27.

Itasca Consulting Group, Inc. (2008). FLAC – Fast Lagrangian analysis of continua, user's manual, www. Itasca.com

Kavazanjian, E., Hushmand, B., & Martin, G. R. (1991). Frictional Base Isolation Using a Layered Soil-synthetic Liner System. In *Proc. 3 US Conf Lifeline Earthquake,* pp. 1140-1151. New York, NY.

Kavazanjian, E., Arab, M., & Matasovic, N. (2012). Performance Based Design for Seismic Design of Geosynthetics-lined Waste Containment Systems. In *Second International Conference on Performance-Based Design in Earthquake Geotechnical Engineering,* Keynote Lecture 19.

Kavazanjian, E., Arab, M., & Matasovic, N. (2013). Performance of Two Geosynthetic-lined Landfills in the Northridge Earthquake. In *7th International Conference on Case Histories in Geotechnical Engineering.* SOAP-5. Chicago, Illinois.

Kavazanjian, E., Jr., Arab, M.G., Fox, P.J. & Matasovic, N. (2014). Performance Based Seismic Design of Geosynthetic Barriers for Waste Containment. In *Earthquake Geotechnical Engineering Design,* M. Maugeri and C. Soccodato (eds.), ISBN 978-3-319-03182-8, Springer-Verlag Berlin Heidelberg, pp. 363-385.

Kutter, B. L. (1992). Dynamic Centrifuge Modeling of Geotechnical Structures. In *Transportation Research Record 1336, TRB, National Research Council*, pp. 24-30. Washington, D.C.

Matasovic, N., & Kavazanjian, E. (1998) Cyclic Characterization of OII Landfill Solid Waste. In Journal of Geotechnical and Geoenvironmental Engineering, 124 (3), pp. 197-210.

Matasovic, N., & Kavazanjian, E. (2006). Seismic Response of a Composite Landfill Cover. In *Journal of Geotechnical and Geoenvironmental Engineering*, Vol. 132, Issue 4, pp. 448-455.

Newmark, N. M. (1965). Effects of Earthquakes on Dams and Embankered Sites. *Rep. No. EERC 72-12.* Earthquake Engineering Research Center, Univ. of California, Berkeley, Calif.

Richardson, G. N., Kavazanjian, E., & Matasovic, N. (1995). RCRA Subtitle D (258) Seismic Design Guidance for Municipal Solid Waste Landfill Facilities. *EPA Guidance Document 600/R-95/051,* U.S. Environmental Protection Agency, Cincinnati.

Safaqah, O., & Riemer, M. (2006). The Elastomer Gage for Local Strain Measurement in Monotonic and Cyclic Soil Testing. In *ASTM Geotechnical Testing Journal,* Vol. 30, No. 2.

Thiel, R., Kavazanjian, E., & Wu, X. (2014). Design Considerations for Slip Interfaces on Steep-wall Liner Systems. In *10th International Conference on Geosynthetics, ICG 2014.*

Thusyanthan, N. I., Madabhushi, S. P. G., & Singh, S. (2005a). Centrifuge Modeling of Solid Waste Landfill Systems-Part 1: Development of a Model Municipal Solid Waste. In *Geotechnical Testing Journal,* Vol. 29, No. 3.

Thusyanthan, N. I., Madabhushi, S. P. G., & Singh, S. (2005b). Centrifuge Modeling of Solid Waste Landfill Systems-Part 2: Centrifuge Testing of Model Waste. In *Geotechnical Testing Journal,* Vol. 29, No. 3.

Wartman, J., Seed, R. B., Bray, J. D., & Rathje E. M. (1999). Laboratory Evaluation of the Newmark Procedure for Assessing Seismically-induced Slope Deformations. In *2nd International Conference on Earthquake Geotechnical Engineering.*

Wartman, J., Seed, R. B., & Bray, J. D. (2001). Shaking Table Experiment of a Model Slope Subjected to a Pair of Repeated Ground Motions. In *4th International Conference on Recent Advances in Geotechnical Earthquake Engineering and Soil Dynamics.*

Wartman, J., Seed, R. B., & Bray, J. D. (2005). Shaking Table Modeling of Seismically Induced Deformations in Slopes. In *Journal of Geotechnical and Geoenvironmental Engineering,* Vol. 131, No. 5, pp. 610-622.

Wilson, D. W. (1998). Soil-Pile-Superstructure Interaction in Liquefying Sand and Soft Clay. PhD dissertation, College of Engineering, University of California: Davis. Davis, California, USA.

Wu, X. (2013). Effect of Waste Settlement and Seismic Loading on the Integrity of Geosynthetic Barrier Systems, MS dissertation, School of Sustainable Engineering and the Built Environment, Arizona State University. Tempe, AZ, USA.

Wu, X (2016). Validation of a Numerical Model for Performance-Based Design of Geomembrane Liner Systems, PhD dissertation in progress (expected completion December 2016), School of Sustainable Engineering and the Built Environment, Arizona State University. Tempe, AZ, USA.

Yegian, M. K., Kadakal, U., & Catan, M. (1999). Geosynthetic for Earthquake Hazard Mitigation. In *Geosynthetics '99: Specifying Geosynthetics and Developing Design Details,* pp. 87-100. Boston, Massachusetts.

APPENDIX A

SUMMARY OF DATA ACQUIRED IN CENTRIFUGE TEST ON GEOMEMBRANE LINED LANDFILL

All of the data collected on this project, including the centrifuge test data and supplemental laboratory testing, as well as the results of the numerical validation analyses, has been archived and is publically available via the Network for Earthquake Engineering Simulation (NEES) project warehouse at https://nees.org/warehouse. Figure A-1 below shows the location of the sensors placed in the centrifuge model. Table A-1 shows the status of each of these sensor. Table A-2 shows the meaning of the codes in Table A-1. Note that in some cases the sensors were installed in redundant pairs: one north of the longitudinal centerline of the model and one south of the longitudinal centerline of the model.

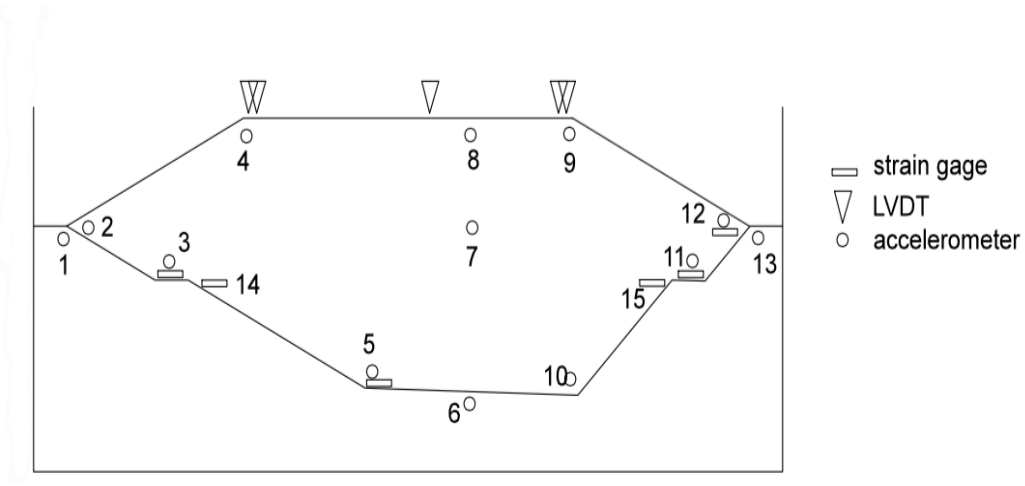

FIG A-1. Centrifuge model sensor locations

Table A-1. Status of centrifuge model sensors throughout the testing program

Sensor	spin-up	motion		
		0.05 g	0.4 g	0.6 g
LVDT				
LP-1 (LPC4)	×	×	×	×
LP-2 (LPC4)	✓	✓	✓	✓
LP-3 (LPC8)	✓	✓	✓	×
LP-4 (LPC9)	✓	✓	✓	✓
LP-5 (LPC9)	×	×	×	×
strain gage				
SA3	✓	✓	×	×
SB3	✓	✓	✓	✓
SC5	×	×	×	×
SA11	✓	×	×	×
SB11	✓	×	×	×
SC12	✓	×	×	×
SC14	×	×	×	×
SC15	✓	×	×	×
accelerometers				
AA1	✓	✓	✓	✓
AA2	✓	✓	✓	✓
AA3	✓	✓	✓	✓
AA4	✓	✓	✓	✓
AA5	✓	✓	✓	✓
AA6	✓	✓	✓	✓
AA7	✓	✓	✓	✓
AA8	✓	✓	✓	✓
AA9	✓	✓	✓	✓
AA10	✓	✓	✓	✓
AA11	✓	✓	✓	✓
AA12	✓	✓	✓	✓
AA13	✓	✓	✓	✓
AB1	✓	✓	✓	✓
AB2	✓	✓	✓	✓
AB3	✓	✓	✓	✓
AB4	✓	✓	✓	✓
AB5	✓	✓	✓	✓

AB6	✓	✓	✓	✓
AB7	✓	✓	✓	✓
AB8	✓	✓	✓	✓
AB9	✓	✓	✓	✓
AB10	✓	✓	✓	✓
AB11	✓	✓	✓	✓
AB12	✓	✓	✓	✓
AB13	✓	✓	✓	✓

Table A-2. Sensor code definition.

CODE	MEANING
LP**	LVDT
S***	Strain gage
A***	Accelerometer
**##	Location in model per Figure A-1
*A**	South of longitudinal centerline
*B**	North of longitudinal centerline
*C**	On longitudinal centerline

APPENDIX B

STRAIN PLOTS

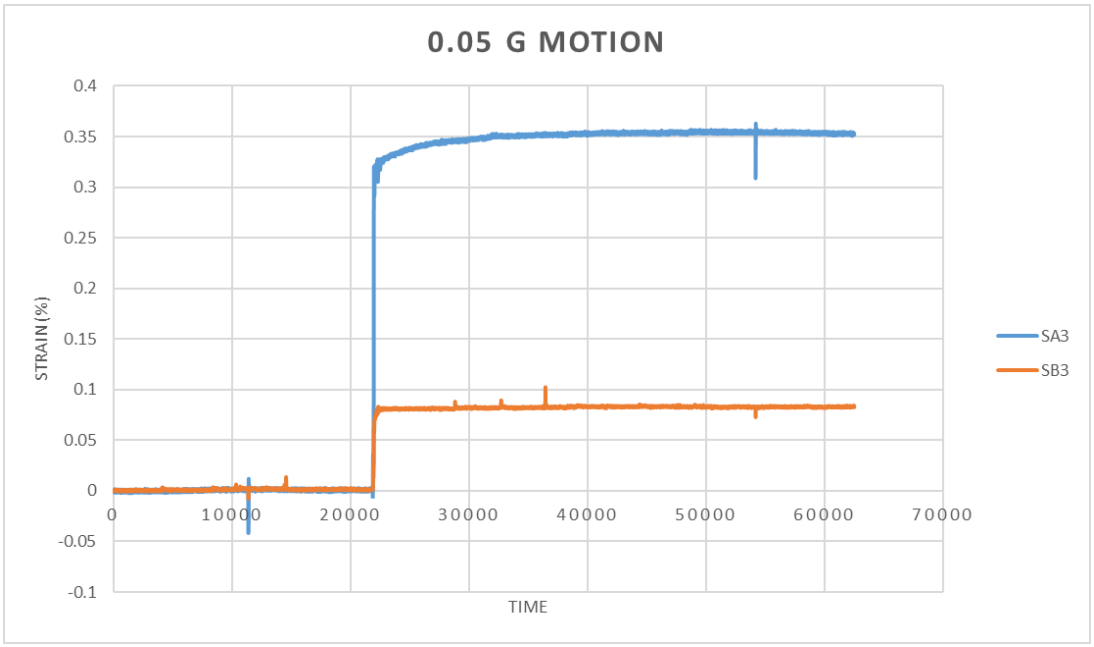
0.05 G MOTION
0.4
0.35
0.3
0.25
0.2
0.15
0.1
0.05
0
-0.05
-0.1
STRAIN (%)
0
10000
20000
30000
40000
50000
60000
70000
TIME
SA3
SB3

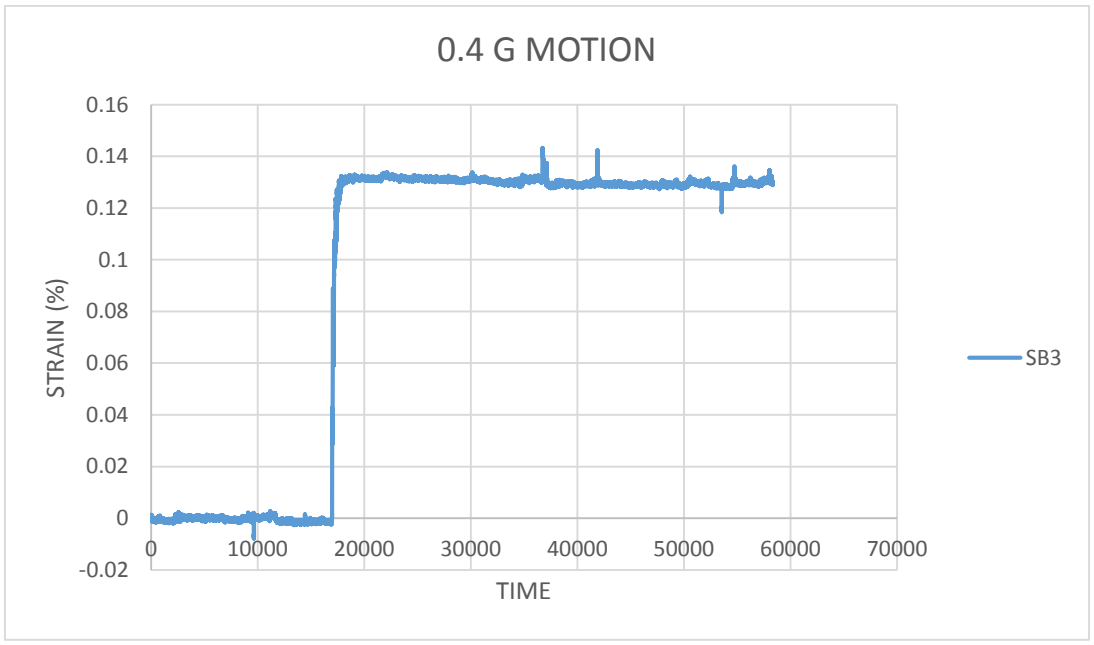
0.4 G MOTION
0.16
0.14
0.12
0.1
0.08
0.06
0.04
0.02
0
-0.02
STRAIN (%)
0
10000
20000
30000
40000
50000
60000
70000
TIME
SB3

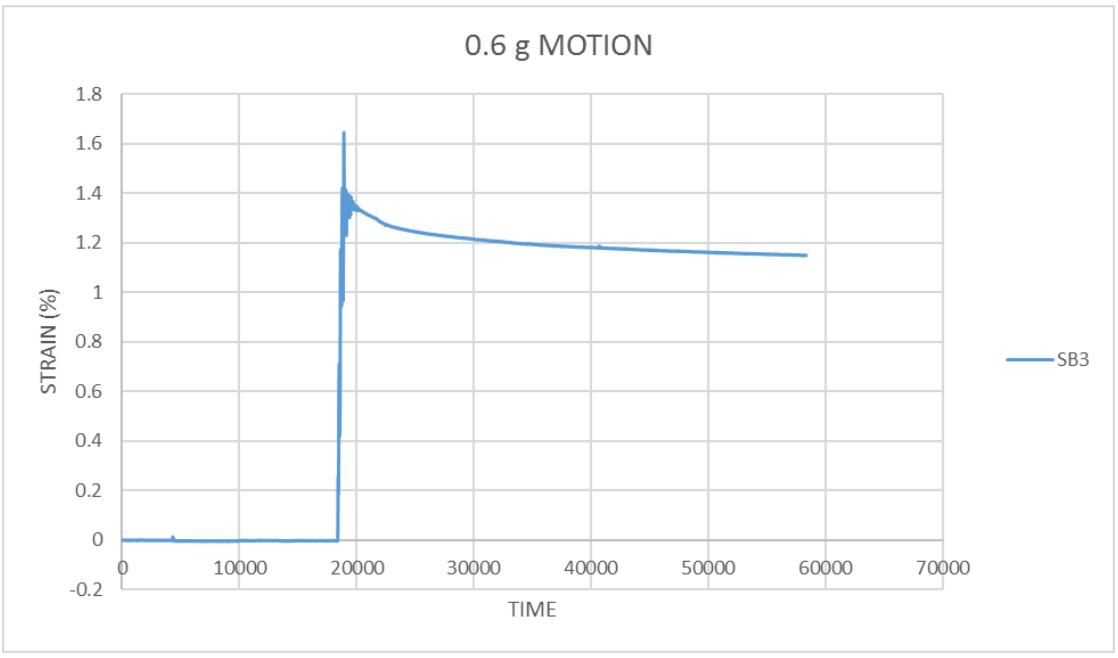
0.6 g MOTION
1.8
1.6
1.4
1.2
1
0.8
0.6
0.4
0.2
0
-0.2
STRAIN (%)
0
10000
20000
30000
40000
50000
60000
70000
TIME
SB3